



# LUND UNIVERSITY

## Dual-layer detector dual energy CT applications for neuroradiology - Spectral brain imaging

Mellander Oxholm, Helena

2025

*Document Version:*

Publisher's PDF, also known as Version of record

[Link to publication](#)

*Citation for published version (APA):*

Mellander Oxholm, H. (2025). *Dual-layer detector dual energy CT applications for neuroradiology - Spectral brain imaging*. [Doctoral Thesis (compilation), Department of Clinical Sciences, Lund]. Lund University, Faculty of Medicine.

*Total number of authors:*

1

### General rights

Unless other specific re-use rights are stated the following general rights apply:

Copyright and moral rights for the publications made accessible in the public portal are retained by the authors and/or other copyright owners and it is a condition of accessing publications that users recognise and abide by the legal requirements associated with these rights.

- Users may download and print one copy of any publication from the public portal for the purpose of private study or research.
- You may not further distribute the material or use it for any profit-making activity or commercial gain
- You may freely distribute the URL identifying the publication in the public portal

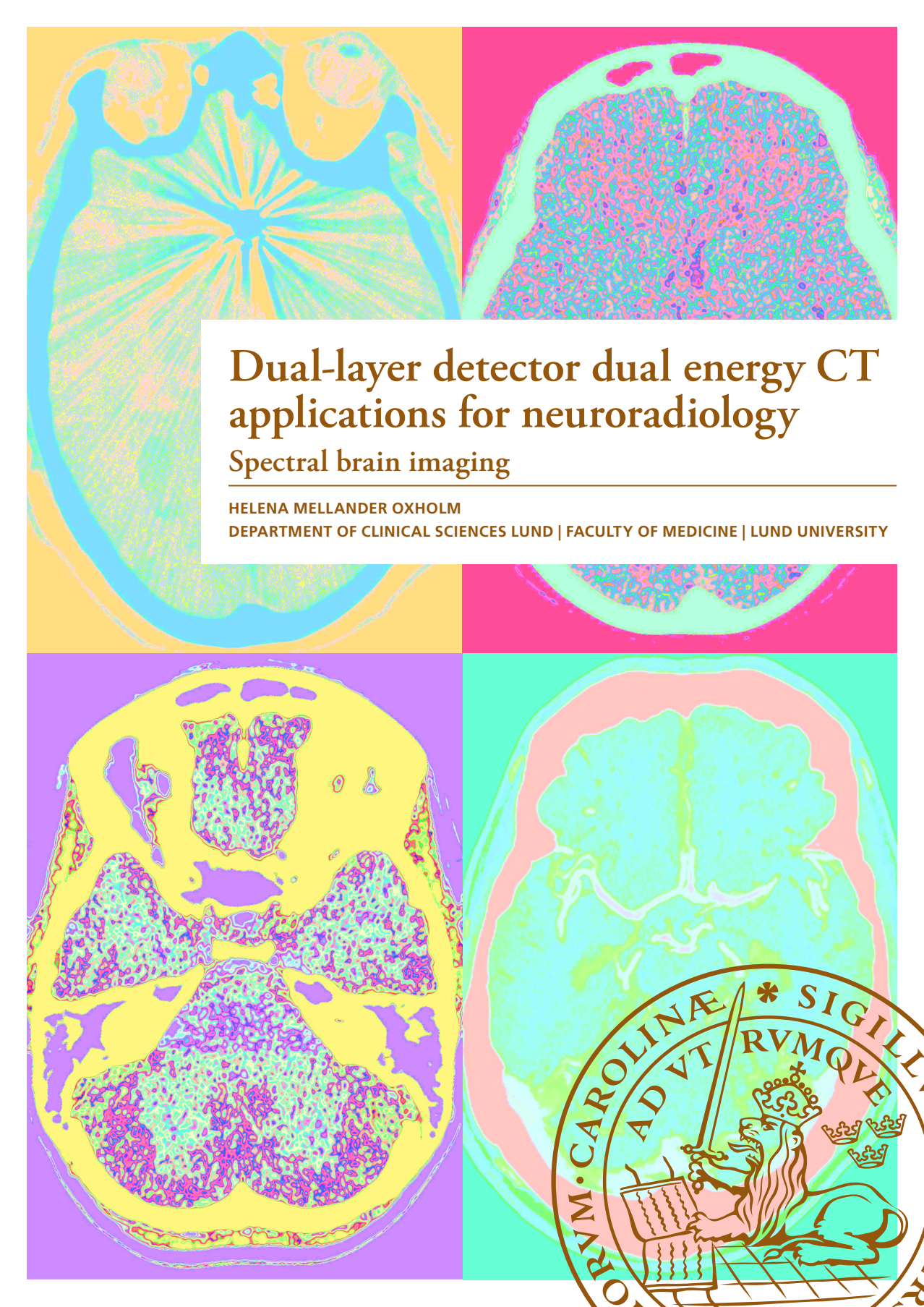
Read more about Creative commons licenses: <https://creativecommons.org/licenses/>

### Take down policy

If you believe that this document breaches copyright please contact us providing details, and we will remove access to the work immediately and investigate your claim.

LUND UNIVERSITY

PO Box 117  
221 00 Lund  
+46 46-222 00 00

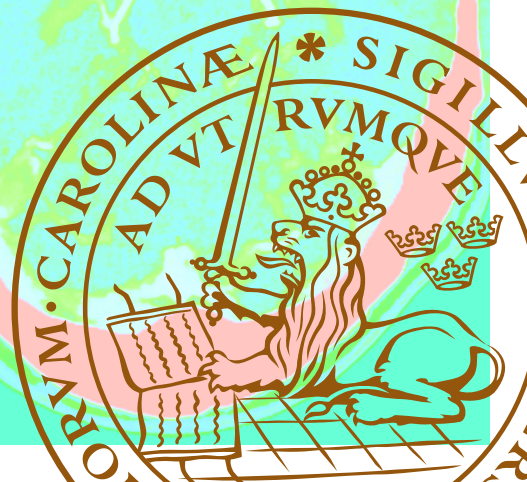


# Dual-layer detector dual energy CT applications for neuroradiology

## Spectral brain imaging

HELENA MELLANDER OXHOLM

DEPARTMENT OF CLINICAL SCIENCES LUND | FACULTY OF MEDICINE | LUND UNIVERSITY



The research behind this thesis was performed with the aim of increasing the knowledge of image quality and the diagnostic value of dual layer detector CT images in neuroradiology. The studies evaluate monoenergetic images in comparison to polyenergetic CT images regarding detection of acute ischemic lesions, reduction of image artifacts and improved enhancement of contrast media.

**HELENA MELLANDER OXHOLM**, M.D., is currently a resident in Radiology at the Department of Medical Imaging and Physiology at Skåne University Hospital in Lund.



Dual-layer detector dual energy CT applications for neuroradiology





# Dual-layer detector dual energy CT applications for neuroradiology

Spectral brain imaging

Helena Mellander Oxholm



**LUND**  
UNIVERSITY

DOCTORAL DISSERTATION

Doctoral dissertation for the degree of Doctor of Philosophy (PhD) at the Faculty of Medicine at Lund University to be publicly defended on 14th of February at 09.00 in Segerfalksalen, Department of Clinical Sciences, BMC, Lund

*Faculty opponent*

Professor Johan Wikström, Akademiska sjukhuset, Uppsala

**Organization:** LUND UNIVERSITY

**Date of issue:** 2025-02-14

Faculty of Medicine

**Document name:** Doctoral Dissertation

Department of Clinical Sciences, Lund

Department of Diagnostic Radiology, Lund

**Author:** Helena Mellander Oxholm

**Title and subtitle:** Dual-layer detector dual energy CT applications for neuroradiology – Spectral brain imaging

## **Abstract**

### **Background:**

Brain CT is a common exam at most hospitals. However, artifacts may reduce the diagnostic value of the exam or the pathologic changes may be hard to visualize in the acute setting. Dual energy CT is an imaging technique that takes advantage of the fact that the attenuation properties of different tissues are dependent on the energy level of the x-rays to which they are exposed. Virtual monoenergetic images may then be created corresponding to images acquired at a chosen energy level. Therefore, it is theoretically possible to improve the diagnostic certainty by using the monoenergetic reconstruction that corresponds to the energy level that best represents the tissue of interest.

### **Methods:**

We have evaluated images acquired by a dual-layer detector spectral CT. All studies (paper I-IV) have been retrospective with patients who had a medical indication for the CT exam. We have collected both objective image data (in predefined areas), calculated image quality parameters (SNR and CNR), and performed subjective analysis by assessment of images by radiologists. Comparisons have been made between conventional polyenergetic images and monoenergetic reconstructions at various energy levels.

### **Results:**

Paper I showed a small reduction of metal artifacts caused by coils. In paper II we showed an improved diagnostic capacity of the addition of monoenergetic images in assessment of acute ischemic lesions. The CTA study showed that it is possible to use a halved dose iodine contrast agent, without affecting exam quality, when assessing low energy VMIs instead of conventional polyenergetic images. In the last project (IV) we found a significant reduction in posterior fossa artifacts in VMIs compared to CIs.

### **Conclusion:**

Monoenergetic images improve the assessment of acute ischemic lesions, evaluation of the posterior fossa and reduce the required dose of iodine contrast administered for CT angiographies. They may also possibly reduce intracranial artifacts by metal implants.

**Key words:** Computed tomography, dual energy, dual-layer detector, CT artifacts, brain CT, ischemic stroke

**Language:** English

**Number of pages:** 83

**ISSN and key title:** 1652-8220 Lund University, Faculty of Medicine Doctoral Dissertation Series 2025:15

**ISBN:** 978-91-8021-668-5

Recipient's notes

Price

Security classification

I, the undersigned, being the copyright owner of the abstract of the above-mentioned dissertation, hereby grant to all reference sources permission to publish and disseminate the abstract of the above-mentioned dissertation.

Signature

Date 2024-01-07

# Dual-layer detector dual energy CT applications for neuroradiology

Spectral brain imaging

Helena Mellander Oxholm



**LUND**  
UNIVERSITY

Cover image by Helena Mellander Oxholm  
Copyright pp 1-83 Helena Mellander Oxholm

Paper 1 © The Authors 2023 (Open Access in European Journal of Radiology Open)  
Paper 2 © The Authors 2022 (Open Access in Acta Radiologica)  
Paper 3 © The Authors 2023 (Open Access in Neuroradiology)  
Paper 4 © The Authors (manuscript not yet published)

Faculty of Medicine  
Department of Clinical Sciences Lund  
Department of Diagnostic Radiology, Lund  
Lund University, Sweden

ISBN 978-91-8021-668-5  
ISSN 1652-8220

Printed in Sweden by Media-Tryck, Lund University  
Lund 2025



Media-Tryck is a Nordic Swan Ecolabel  
certified provider of printed material.  
Read more about our environmental  
work at [www.mediatryck.lu.se](http://www.mediatryck.lu.se)

**MADE IN SWEDEN** 



*The only impossible journey is the one you never begin*

# Table of Contents

Abbreviations .....	10
Abstract .....	12
Thesis at a glance .....	13
Populärvetenskaplig sammanfattning.....	14
List of papers.....	17
Author's contributions to papers I-IV .....	19
<b>Introduction .....</b>	<b>21</b>
A brief history of computed tomography .....	21
CT physics and technique .....	23
What are x-rays?.....	23
The components of a modern CT .....	25
Dual energy CT .....	26
Creating the images (postprocessing).....	32
The sinogram.....	32
Types of reconstruction .....	32
Filters.....	33
Reconstructing dual energy images.....	33
Image quality.....	35
Image contrast .....	36
Noise.....	36
Image resolution .....	37
Artifacts .....	37
Measures of image quality.....	38
CT in neuroradiology .....	40
Stroke Imaging .....	41
Image artifacts in neuroradiology.....	43
CT contrast medium.....	44
<b>Aims .....</b>	<b>47</b>
<b>Materials and methods.....</b>	<b>49</b>
Paper I .....	51

Paper II .....	52
Paper III.....	53
Paper IV .....	54
Statistical analysis .....	55
Ethical considerations .....	55
<b>Results.....</b>	<b>57</b>
Paper I .....	57
Paper II .....	59
Paper III.....	60
Paper IV .....	61
<b>Discussion .....</b>	<b>63</b>
What are conventional images?.....	63
Exam radiation doses .....	64
Evaluation of image quality .....	64
Quantitative measures .....	64
Qualitative measures .....	65
CT angiography.....	66
The use of VMIs.....	67
Strengths and limitations.....	67
Clinical impact .....	68
<b>Conclusions .....</b>	<b>69</b>
<b>Moving forward .....</b>	<b>71</b>
<b>Acknowledgements .....</b>	<b>73</b>
<b>References .....</b>	<b>75</b>

## Abbreviations

ACA	Anterior cerebral artery
ASPECTS	Alberta Stroke Program Early CT Score
AUC	Area under the curve
CI	Conventional images
CNR	Contrast-to-noise ratio
CM	Contrast medium
CT	Computed tomography
CTA	CT angiography
CTDI	Computed tomography dose index
DLP	Dose-length product
DECT	Dual energy CT
DLCT	Dual-layer detector CT
FBP	Filtered back projection
FOV	Field of view
HU	Hounsfield units
GM	Grey matter
ICA	Internal carotid artery
IGM	Ischemic grey matter
IR	Iterative reconstruction
keV	Kiloelectron volt
kVp	Peak kilovoltage
LVO	Large vessel occlusion
MAR	Metal artifact reduction
MCA	Middle cerebral artery
MRI	Magnetic resonance imaging
NCCT	Non-contrast CT
NGM	Normal grey matter
NWM	Normal white matter

ROC	Receiver operating characteristics
ROI	Region of interest
SBI	Spectral base image
SD	Standard deviation
SNR	Signal-to-noise ratio
PFAI	Posterior fossa artifact index
PACS	Picture archiving and communication system
PCA	Posterior cerebral artery
prASPECTS	posterior circulation Acute Stroke Prognosis Early CT Score
VMI	Virtual monoenergetic image
VNC	Virtual non-contrast
WM	White matter



# Abstract

## Background

Brain computed tomography (CT) is a common exam at most hospitals. However, artifacts may reduce the diagnostic value of the exam or the pathologic changes may be hard to visualize in the acute setting. Dual energy CT is an imaging technique that takes advantage of the fact that the attenuation properties of different tissues are dependant on the energy level of the x-rays to which they are exposed. Virtual monoenergetic images (VMIs) may then be created corresponding to images acquired at a chosen energy level. Therefore, it is theoretically possible to improve the diagnostic certainty by using the monoenergetic reconstruction that corresponds to the energy level that best visualizes the tissue of interest.

## Methods

We have evaluated images acquired by a dual-layer detector dual energy CT. All studies (Papers I-IV) have been retrospective and thus included patients who had a medical indication for the CT exam. We have collected both quantitative image data (in predefined areas), calculated image quality parameters (such as signal-to-noise and contrast-to-noise ratio), and performed qualitative analysis by assessment of images by radiologists. Comparisons have been made between conventional polyenergetic images and monoenergetic reconstructions at various energy levels.

## Results

Paper I showed a small reduction of metal artifacts caused by coils in monoenergetic images compared to conventional images. In paper II we showed an improved diagnostic capacity with the addition of monoenergetic images for assessment of acute ischemic lesions. The CT angiography study (paper III) showed that it is possible to use a halved dose iodine contrast agent, without affecting the exam quality, when assessing low energy VMIs instead of conventional polyenergetic images. In the last project (IV) we found a significant reduction in posterior fossa artifacts in VMIs compared to CIs.

## Conclusion

Monoenergetic images improve the assessment of acute ischemic lesions, evaluation of the posterior fossa and reduce the required dose of iodine contrast administered for CT angiographies. They may also possibly reduce intracranial artifacts by metal implants.

## Thesis at a glance

Study	Aim	Methods	Results	Conclusion
I	To quantitatively and qualitatively investigate the potential reduction of intracranial metal artifacts by coils in virtual monoenergetic images (VMIs) by dual-layer detector CT (DLCT) compared to conventional images (CIs).	Retrospective inclusion of 32 consecutive patients examined with a DLCT and collection of mean Hounsfield units (HU) and standard deviation in predefined locations both with and without artifacts. Qualitative grading of image quality.	In artifact affected tissue distal to the metal coils the mean attenuation value decreased with higher energy level VMIs. Overall image quality scores were significantly higher in VMIs at 60 and 70 keV compared to CIs.	There is a small significant reduction of intracranial coil artifact severity by monoenergetic reconstructions with preserved or increased overall image quality compared to conventional images.
II	To evaluate whether the ability to detect acute cortical ischemic lesions is improved in DLCT virtual monoenergetic reconstructions compared to CIs.	Using a cohort of patients with a confirmed cortical ischemic lesion, we investigated image quality and tissue contrast. We also included exams without lesions to perform tests of diagnostic accuracy.	Tissue contrast between normal white and ischemic grey matter was higher in VMIs at 40-70 keV compared to CIs. The sensitivity for diagnosing acute ischemic lesions was higher when adding VMIs to the assessment.	VMIs may improve the diagnostic ability in by enhancing tissue contrast with may improve the radiological accuracy in assessment of acute ischemic lesions.
III	To investigate whether image quality can be preserved in brain CTA with halved contrast dose by using VMIs and to investigate whether VMIs can compensate for poor arterial enhancement.	Consecutive adult patients examined with a CTA with either full contrast dose or halved contrast dose with suboptimal or optimized timing. HU values were collected in predefined areas. Visual grading of CTA quality was performed.	Both quantitatively and qualitatively VMIs at 40-60 keV improved image quality. The VMIs at 50 keV in the exams performed with halved contrast dose and optimized timing received significantly higher qualitative ratings than the CIs of the exams performed with full contrast dose.	Using a halved dose contrast and 50 keV reconstructions the image quality is greater compared to CIs with full contrast dose. Using VMIs may also increase the number of diagnostic examinations.
IV	To evaluate posterior fossa artifacts in VMIs by a spectral dual-layer detector CT compared with conventional polyenergetic images.	Inclusion of patients with CT brain exams that had been assessed as normal. Measurements and image parameters were collected and a visual grading of both CIs and VMIs was performed.	The noise levels were significantly lower in the posterior fossa in VMIs $\geq 60$ keV compared to CIs. VMIs at 60 keV received the highest qualitative scores for overall image quality and posterior fossa artifacts.	Artifacts in the posterior fossa are reduced in VMIs compared to CIs with an improved overall image quality.

## Populärvetenskaplig sammanfattning

Skiktröntgen (CT) av hjärnan är en vanlig bilddiagnostisk undersökning och exempel på de frågor som dessa undersökningar ämnar besvara kan vara rörande s.k. ischemisk infarkt (infarkt i hjärnan orsakad av en blodpropp), blödning, svullnad i hjärnvävnaden eller uppföljning efter operationer.

Skiktröntgen har många fördelar, bland annat är det en relativt billig undersökning då den går snabbt att utföra. Skiktröntgen är också oftast lättillgängligt, dvs finns på de flesta sjukhus och kan ofta köras dygnet runt (jämfört med tex magnetkameraundersökningar som tar längre tid och ofta är ytterst begränsade utanför ordinarie arbetstider).

Det finns dock även nackdelar med skiktröntgen, exempelvis så kan bildernas värde begränsas av artefakter (t.ex. streck i bilderna) orsakade av t.ex. metallimplantat eller det tjocka skallbenet, vilket kan försvåra bedömningen avseende t.ex. små blödningar eller ischemiska infarkter. Vid en misstänkt infarkt i hjärnan (s.k. stroke), utförs ofta en skiktröntgen så fort som möjligt men infarkter orsakade av blodproppar kan på en konventionell skiktröntgen vara mycket svåra att avgränsa i ett tidigt skede. Syftet med undersökningen blir då snarare att utesluta en annan orsak till patientens symtom (så som blödning) och om sådan inte kan påvisas riskerar diagnosen att bli osäker. En annan nackdel med skiktröntgen är att i vissa fall vill man förstärka bilderna med s.k. kontrastmedel vilket ofta utgörs av en jodbaserad vätska som patienten får via en spruta in i blodomloppet. Denna jodbaserade vätska kan dock vara skadlig för njurarna, särskilt för patienter som redan har en nedsatt njurfunktion sedan tidigare.

Traditionellt baseras skiktröntgenbilder på hur röntgenstrålar med ett spektrum av olika energier passerar genom ett objekt (en patient) och träffar en detektor, dessa bilder kan kallas *polyenergetiska* bilder just eftersom strålarna har många olika energier. Bilderna som sedan skapas i en skiktröntgen motsvarar det avbildade objektets täthet.

Olika vävnadstyper avbildas dock olika väl beroende på strålarnas energi men om man kan separera strålarna och sortera dem beroende på dess energi så kan man skapa så kallade *monoenergetiska* bilder. Beroende på vad man vill titta på så kan man därefter välja den monoenergetiska bilden med mest lämpad energinivå och möjligen på så sätt förbättra undersökningens diagnostiska kapacitet (dvs hur säkert röntgenläkaren kan påvisa eller utesluta ett tillstånd). Med s.k. 'spektral-CT' eller 'dubbelenergi-CT' kan sådana monoenergetiska bilder skapas. Som ett exempel på detta, så kan avbildningen av jod (som finns i kontrastmedel) förstärkas i monoenergetiska bilder gjorda på lägre energinivåer (teoretiskt ca 30 kiloelektronvolt) och möjligen kan man då sänka mängden kontrastmedel och därmed spara njurfunktion om man tittar på monoenergetiska bilder på rätt nivå i

stället för på de polyenergetiska bilderna (som får en högre medelenergi än den som är optimal för visualisering av jod).

I den första studien ville vi ta reda på om artefakter från metallimplantat kan minskas med hjälp av monoenergetiska jämfört med polyenergetiska bilder. Vi inkluderade patienter med s.k. coils (metallnystan som används vid behandling av vissa kärlförändringar i hjärnan) som undersökts med spektral-CT. Vi utförde mätningar i bilderna, både på polyenergetiska bilder och i monoenergetiska bilder på olika energinivåer. Vi lät också radiologer visuellt bedöma och poängsätta bildkvaliteten på de olika sorters bilderna. Resultaten visade att en viss minskning av metallartefakter kan erhållas i monoenergetiska bilder vilket därmed kan förbättra undersökningsvärdet för patienter som har behandlats med coils.

I den andra studien undersökte vi huruvida tidiga tecken till infarkt orsakad av en blodpropp (ischemisk stroke) syns bättre på så kallade monoenergetiska skiktröntgenbilder än på polyenergetiska bilder. På traditionella skiktröntgenbilder är dessa förändringar nämligen svåra att avgränsa i ett tidigt skede och diagnosen blir därmed ibland osäker. I studien inkluderade vi patienter där senare undersökningar (skiktröntgen eller magnetkamera) bekräftat förekomsten av en ischemisk skada. Vi kunde då exakt lokalisera det drabbade området på den första skiktröntgenundersökningen (utförd inom 12 h efter insjuknande) och utföra mätningar av vävnadstäthet och brus i bilderna. Vi inkluderade också bilder på hjärnor utan ischemisk skada och lät röntgenläkare titta på alla fallen (både poly- och monoenergetiska bilder) och svara på huruvida det fanns en ischemisk skada eller inte. Resultaten visade att fler av de positiva fallen (med stroke) kunde diagnostiseras korrekt med hjälp av monoenergetiska bilder jämfört med bara polyenergetiska bilder. Vi hittade också ett generellt lägre signal/brus-förhållande i de monoenergetiska bilderna jämfört med de polyenergetiska, detta kan tolkas som en bättre bildkvalitet.

I den tredje studien ville vi ta reda på om det, med bibehållen bildkvalitet, går att sänka dosen kontrastmedel i samband med skiktröntgen av hjärnans artärer. Vi inkluderade patienter som skulle undersökas med en artärinriktad dubbelenergiskiktröntgen av hjärnan och körde undersökningar där vi bland annat halverade kontrastdosen. Vi utförde mätningar av kontrastfyllnaden på förbestämda platser i hjärnans kärl och jämförde skillnaden mellan täthet i kärlen och hjärnparenkymet för både poly- och monoenergetiska bilder. Vi lät också röntgenläkare granska och poängsätta bilderna avseende bland annat hur väl kärlen avbildats. Studien visade att det går att halvera mängden kontrastmedel med bibehållen, eller till och med förbättrad, bildkvalitet om man använder monoenergetiska bilder.

I den fjärde studien, som är utförd men ännu inte är publicerad, ville vi utvärdera artefakter i den bakre delen av skallen (den bakre skallgropen). Dessa artefakter orsakas av det täta skallbenet och orsakar streck i bilderna. Vi utförde mätningar av

täthet och brus på fördefinierade ställen i hjärnan och jämförde sedan de mono- och polyenergetiska bilderna. Röntgenläkare fick poängsätta bilderna avseende generell bildkvalitet, artefakter och hur väl det gick att skilja på olika sorters vävnad i hjärnan. Studien visar att monoenergetiska bilder har generellt högre signal/brusförhållande (vilket indikerar in lägre artefaktgrad/bättre bildkvalitet) och bättre kontrast mellan olika sorters vävnad i hjärnan. Monoenergetiska bilder fick de högsta betygen både avseende artefaktutbredning och generell bildkvalitet.

Resultaten i dessa studier kan förhoppningsvis bidra till en ökad förståelse för hur vi skapar så bra bilddiagnostiska undersökningar som möjligt vilket är en stor vinst för både patienterna och för sjukvården som en helhet.



# List of papers

The thesis is based primarily on the following papers which are appended in the end of the thesis.

## *Paper I*

**Mellander H**, Fransson V, Ydström K, Lätt J, Ullberg T, Wassélius J, Ramgren B. Metal artifact reduction by virtual monoenergetic reconstructions from spectral brain CT. *Eur J Radiol Open*. 2023 Feb 3;10:100479. DOI: 10.1016/j.ejro.2023.100479. eCollection 2023.

## *Paper II*

**Mellander H**, Bengtsson P, Fransson V, Ramgren B, Undrén P, Drake M, Ydström K, Lätt J, Hilal A, Wassélius J, Ullberg T. Virtual monoenergetic images by spectral detector computed tomography may improve image quality and diagnostic ability for ischemic lesions in acute ischemic stroke. *Acta Radiol*. 2023 Apr;64(4):1631-1640. DOI: 10.1177/02841851221130612. Epub 2022 Oct 18.

## *Paper III*

Fransson V, **Mellander H**, Ramgren B, Andersson H, Arena F, Ydström K, Ullberg T, Wassélius J. Image quality of spectral brain computed tomography angiography using halved dose of contrast medium. *Neuroradiology*. 2023 Sep;65(9):1333-1342. DOI: 10.1007/s00234-023-03190-1. Epub 2023 Jul 15.

## *Paper IV*

**Mellander H**, Fransson V, Hansen B, Ramgren B, Ydström K, Ullberg T, Wassélius J. Reduction of posterior fossa artifacts using spectral monoenergetic CT images. Manuscript submitted to *Neuroradiology* in November 2024.

Additional original publications not included in this thesis:

**Mellander H**, Hilal A, Ullberg T, Wassélius J. Evaluation of CINA® LVO artificial intelligence software for detection of large vessel occlusion in brain CT angiography. *Eur J Radiol Open*. 2023 Dec 15;12:100542. DOI: 10.1016/j.erjo.2023.100542. eCollection 2024 Jun.

Fransson V, **Mellander H**, Wassélius J, Ydström K. Detection of perfusion deficits in multiphase computed tomography angiography – A stroke imaging technique based on iodine mapping on spectral computed tomography: Initial findings. *J Comput Assist Tomogr*. 2021 Jul-Aug 01;45(4):618-624. DOI: 10.1097/RCT0000000000001173.

Lehti L, Söderberg M, **Mellander H**, Wassélius J. Iterative metal artifact reduction in aortic CTA after Onyx<sup>®</sup>-embolization. Eur J Radiol Open. 2020 Sep 4;7:100255. DOI: 10.1016/j.erjo.2020.100255. eCollection 2020.

## Author's contributions to papers I-IV

### *Paper I*

For this paper I suggested the methodology and wrote the final project plan. I collected the quantitative data and took part in setting up the software for collection of the qualitative data. I analysed the main part of both the quantitative and qualitative data and wrote the first draft of the manuscript.

### *Paper II*

I revised the project plan and methodology and collected all of the quantitative data. I analysed both the quantitative and qualitative data and created the figures. I performed the statistical analysis. I wrote the first draft of the manuscript and was active in both revision of the manuscript and in writing a response to reviewers.

### *Paper III*

For this paper I worked with another PhD-student (first author Veronica Fransson) in suggesting the methodology and in collecting the quantitative data. I reviewed and edited the draft of the manuscript.

### *Paper IV*

I suggested the study design/methodology, collected the objective data and set up the software for collection of the qualitative data. I analysed both the quantitative and qualitative data, created the figures and performed the statistical analysis. I wrote the first draft of the manuscript.



# Introduction

The following sections aim to introduce the relevant knowledge behind Paper I-IV and will therefore introduce the reader to CT physics and technique, measurements of image quality and, through the clinical perspective, why this can be important for our patients.

## A brief history of computed tomography

In the early 1960s the South African physicist Alan Cormack (Figure 1) published a mathematical solution to calculate attenuation coefficients in a cylindrical phantom containing wood and aluminium by measuring parallel transmissions through the phantom [1, 2]. His main interest for this was in regard to improving the calculations of radiation doses in radiotherapy which at the time were estimated by radiographs and calculated as if the patients were homogenous [3, 4]. While introducing the reader to the lack of knowledge of separating different tissues, using conventional radiography that was in clinical use at the time, Cormack stated in his 1963 publication:

“It is sufficient to consider the problem in two dimensions, since, if a solution can be found for two dimensions, the three-dimensional case may be solved by considering it to be a succession of two-dimensional layers”

However, at the time Cormack’s work gained little response.

Also in the 1960s, the English electrical engineer Godfrey Hounsfield (Figure 1) worked on differentiation of different tissues by data from a set of angles in a two-dimensional model (initially a 3 x 3 grid in 1967). Despite little support and engagement by radiologists at the time (the belief seemed to be that the image quality never could be sufficient), Hounsfield carried on his work and met the British neuroradiologist Dr James Ambrose who demonstrated some of the common neuroradiological exams at the time, after which Hounsfield stated, “*I can do much better than that*”. Their collaboration led to the first clinical CT brain exam performed in October 1971 at the Atkinson Morley Hospital in England. The reconstructions of the 80 x 80-pixel exam took twenty minutes per image slice but clearly visualized the suspected frontal lobe tumour in the patient’s brain [4-7]. The



CT was displayed at the annual RSNA (Radiological Society of North America) meeting in 1972, and the production of this first clinical CT machine (The EMI Mark I scanner) started the same year with machines being set up in the USA and in the UK [4, 8, 9]. Hounsfield kept on his work on improving CT long after this.

Alan Cormack and Godfrey Hounsfield shared the Nobel Prize in Physiology or Medicine in 1979 for their contributions in the development of the computer-assisted tomography. In his Nobel Laureate lecture Cormack described that many years after his publications he had found out that the mathematical problem had already been solved in 1917 by the Austrian physicist Johann Radon (the *Radon transform*) who thus actually was the first to lay the mathematical foundation (the Radon transform) of the CT technique [10]. Johann Radon should therefore also be given due credit, even though Cormack came up with his solution unknowingly of Radon's 1917 publication. Many others who contributed have not been mentioned but there are several in depth descriptions of the development of the CT available [3, 4, 7, 11, 12].



**Figure 1.**

Allan M. Cormack in 1984 (left) and Godfrey N. Hounsfield in 1975 (right). The picture of Allan Cormack is distributed under the CC-BY 3.0. <http://creativecommons.org/licenses/by/3.0>

The picture of Godfrey Hounsfield is considered public domain by The National Library of Medicine and to the authors knowledge under no copyright.

Since the first computed tomograph was introduced, the technique has been ever evolving. The first CT similar to currently used models, with a simultaneously rotating tube and detector came in 1975 and since then two major developments in CT technology will be briefly mentioned.

First, the ‘spiral technique’ with a continuously rotating gantry while, at the same time, moving the patient through the x-ray beam was introduced in 1989 and drastically reduced the scan times and hence, reduced motion artifacts.

Second, multidetector-rows were introduced around the 2000s and successively increased total detector width and thereby increased the scanned area per gantry rotation to now up to about 16 cm. This also resulted in a major reduction of scan time [12, 13].

Some more current developments include dual energy CT and photon counting detectors. The principles of dual energy CT is described in the next section.

## CT physics and technique

### What are x-rays?

Generally, atoms have a neutral charge in their natural state i.e. the number of protons is the same as the number of electrons. However, atoms may be ‘ionized’ (positively or negatively charged) if, for example, enough energy is deployed in one of the electrons so that it is removed from the atom (which then becomes positively charged). The electrons can also jump to outer shells if the appropriate amount of energy is deployed – the electron is ‘excited’.

X-rays are electromagnetic waves, small, moving energy units (photons), just like visible light but with higher energies and hence shorter wavelengths (Figure 2). X-rays are widely used in medical imaging, were first discovered by Wilhelm Röntgen in 1895 [14] and have been increasingly used since conventional radiography, fluoroscopy and thereafter CT have been introduced.

X-rays may be created by rapid acceleration of electrons from a cathode to an anode (negatively and positively charged respectively) by placing a high potential between them (usually around 120 kV). The electrons can cause either ionization or excitation in the material (usually wolfram) in the anode, this creates empty spaces in the electron shells. These spaces that are then filled out by electrons from outer shells and the difference in energy is released as electromagnetic radiation called *characteristic x-rays*. The accelerated electrons can also interact with the nucleus of the wolfram atoms, which results in a course change and deceleration of the electrons, in this process energy is released as *breaking radiation* (bremsstrahlung). [15, 16].

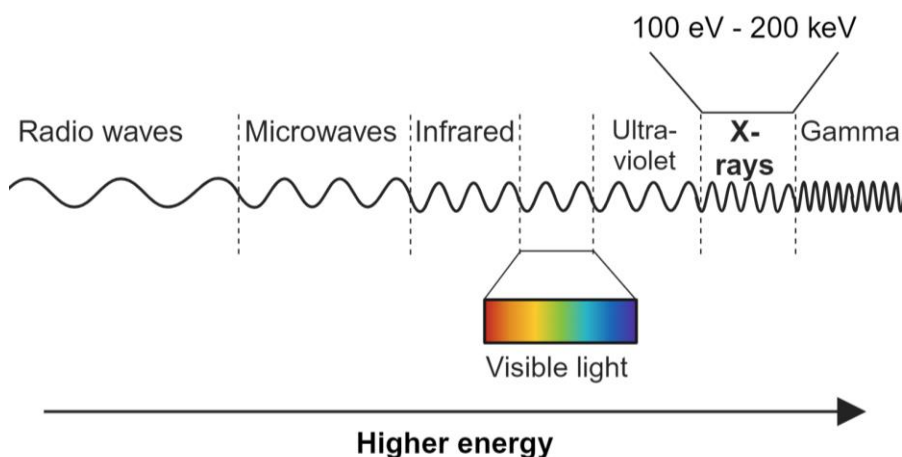


**Figure 2.**

Illustration of the electromagnetic spectrum depending on energy level. X-rays have high energies (compared to visible light) at approximately 0,1 to 200 kiloelectron volts (keV). Image created in biorender.com.

X-rays that are used in medical imaging mainly consist of braking radiation and characteristic x-rays at a spectrum of different energies [17]. X-rays have energies of about 0,1 to 200 kiloelectron volts and the maximum energy of the x-rays depend on the peak potential (peak kilovoltage, kVp) of the x-ray tube.

When the x-rays then reach the patient, they can either: pass through unaltered, interact with electrons in the atoms in the tissue causing ionization or excitation, or collide with electrons in the tissue which results in a loss of energy and an altered course of the x-ray.

As we know, ionization or excitation results in the production of characteristic x-rays - this process is called the *photoelectric effect* and in this case all of the photon's energy is lost. The course change and loss of energy is called *Compton scatter* (or the Compton effect). The type of interaction that is predominant, the photoelectric effect or Compton scatter, depends on the energy of the X-rays, the atomic numbers within the tissue and, the electronic density of the tissue. The photoelectric effect is highly energy dependant (more predominant in lower energies) and dependant of the atomic number of the tissue (with higher atomic numbers within the tissue the higher the proportion of the attenuation will be due to the photoelectric effect). Compton scatter is less energy dependant (occurs at energies > 50 keV) compared to the photoelectric effect but dependant on the electronic density of the tissue (which in turn is dependent on the atomic number and number of atoms within a volume) [15, 17-19]. In turn, the energy spectrum of the x-rays depends on the peak tube potential (kVp) used in the x-ray source. These differences are the key to dual energy CT imaging.

These interaction between the x-rays and the tissues in the patients together cause an *attenuation* of the x-ray spectrum when passing through the object, this means that an altered number of x-rays, with an altered spectrum of energies, reach the detector where they are registered after being converted to visible light.

The absorption values in each image element (voxel) are measured in Hounsfield units (HU) which corresponds to the tissue's density normalized against the attenuation of water (0 HU) and air (-1000 HU) [20].

## The components of a modern CT

The *x-ray tube* (source) is made up of a cathode and an anode, and when a high potential is placed between them x-rays are created in the anode as described in the previous section. After the x-rays have been produced, *collimators* focus the x-rays in the patient's length axis ('Z-axis') and limit the size of the x-ray field thus determining how many of the detector rows that are used. *Filters* are placed through the x-ray beam to remove x-rays with insufficient energy to contribute to image data, these low energy x-rays would otherwise only add on the radiation dose to the patient (the skin dose).

The detector usually has an *anti-scatter grid* which consists of parallel lines of high-density material (such as lead) to filter out the x-rays that come towards the detector at too low angles, these x-rays are created by scattered radiation from the patient and reduce image quality (Figure 3).

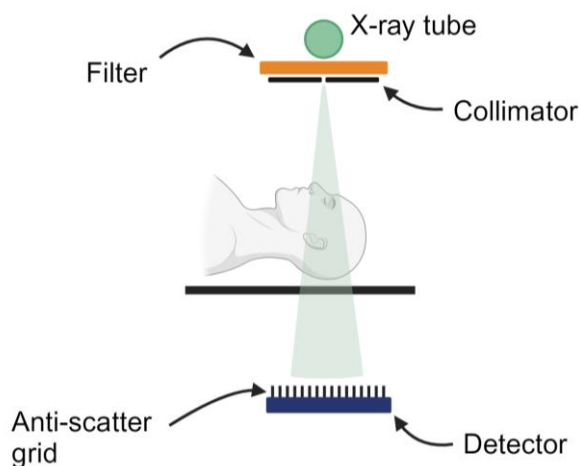


**Figure 3.**

Illustration of some essential components in a CT: The *x-ray tube* in which the x-rays are produced, one or more *filters* to customize the x-ray beam, a *collimator* to limit the x-ray field, an *anti-scatter grid* preventing scattered radiation of reaching the detector and, the *detector* which registers the incoming x-rays. Image created in biorender.com.

Standard *detectors* (Figure 4) are currently made up of one layer of a *scintillator*, a crystal layer made of for example gadolinium oxysulfide, in which the incoming x-rays are converted into visible light. Surrounding each detector element are reflective walls placed to reduce scatter between detector elements. The visible light created in the scintillator is then detected by photodiodes in the bottom of the detector, is then either directly converted into a digital signal or is first transferred into an electric signal which is then converted to a digital signal. Current detectors have detector elements with an area of about 0,5x0,5 mm and detectors are made up of multiple rows of detector elements (usually 64 rows in a 4 cm (Z-axis) detector). How these elements are configured is part in determining the minimal slice thickness, and the total detector width limits how long a volume of the patient can be scanned in one rotation [17, 21-23].

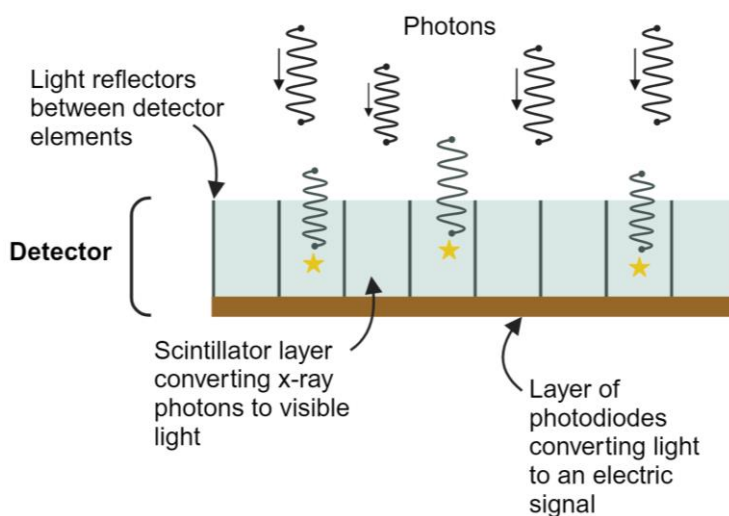


**Figure 4.**

Illustration of the components of a standard CT detector. The x-ray photons are converted to visible light when hitting the scintillator layer, the light remains in the specific detector element since the sides of the element are made up of a light reflective material. The light is transformed into an electric signal via photodiodes at the bottom of each detector element. Image created in biorender.com.

## Dual energy CT

“Two pictures are taken of the same slice, one at 100 kV and the other at 140 kV. If the scale of one picture is adjusted so that the values of normal tissue are the same on both pictures, then the picture containing material with a high atomic number will have higher values at the corresponding place on the 100 kV picture”

Already in 1973 Sir Godfrey Hounsfield stated the above in his publication *Computerized transverse axial scanning (tomography): Part 1 Description of*

system [5]. The statement and the knowledge behind it lays the foundation of dual energy CT (DECT) and as such, long before technology was able to handle dual energy data, the theory behind it was known and suggested as a promising future aspect in medical imaging.

It was first in 2006 that the first dual energy system (SOMATOM Definition by Siemens Healthineers), a dual source system, was launched [24]. Currently however, there are several available dual energy CT systems on the market, the type of technology used to acquire the dual energy data is usually manufacturer dependent and the technologies are described below.

The basic physics behind dual energy is, as stated above, the fact that different elements have characteristic attenuation curves, i.e. they attenuate the x-rays differently depending on the energy of the x-rays. The attenuation is dependent on the atomic number of the element in question and the higher the atomic number - the higher the attenuation in lower energy images. The *k-edge* in the specific attenuation curve is a sudden increase in attenuation at a certain energy level, this corresponds to the energy level needed for ejection of electrons in the K-shell of the atom in question, which results in an increase in the attenuation by the photoelectric effect.

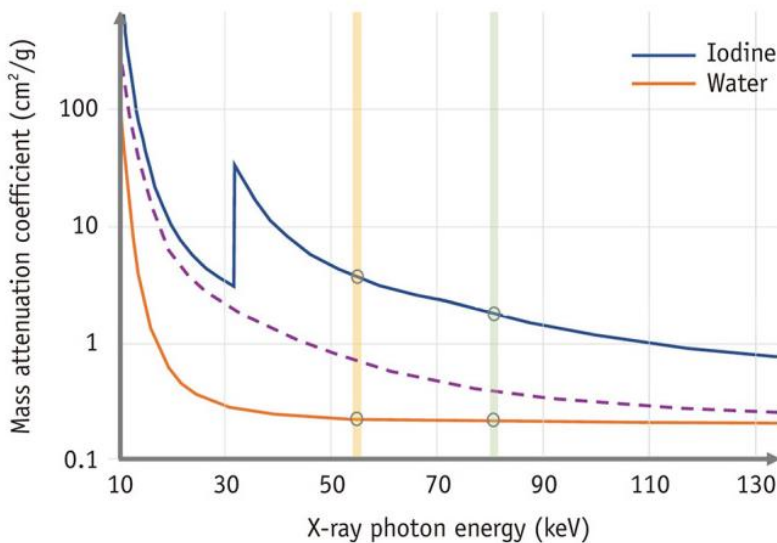


**Figure 5.**

Attenuation curves of iodine and water at photon energies from 10 to 130 keV. Original figure from *Spectral Computed Tomography: Fundamental Principles and Recent Developments* by Aaron So and Savvas Nicolaou. ©2021 The Korean Society of Radiology. Figure distributed under the CC BY-NC 4.0 <http://creativecommons.org/licenses/by-nc/4.0>.

If you can identify the attenuation curve for a pixel in an image and it corresponds to the known attenuation curve of a specific element it is possible to identify the tissue or element in that image pixel. For example, iodine has a specific attenuation curve (Figure 5), with a k-edge at 33 keV which makes it possible to identify iodine if there is data at, at least, two different energy levels [5, 11, 25].

Different ways to acquire dual energy data and images have been developed by different manufacturers. For example, dual energy data can be acquired by performing two separate scans at different kVp levels, there are systems based on rapid kVp switching during the scan, dual source techniques using x-rays tubes at different energy level and two separate detectors and, a dual-layer detector system, where the x-rays are separated as high or low energy by different layers of the detector (Figure 6).

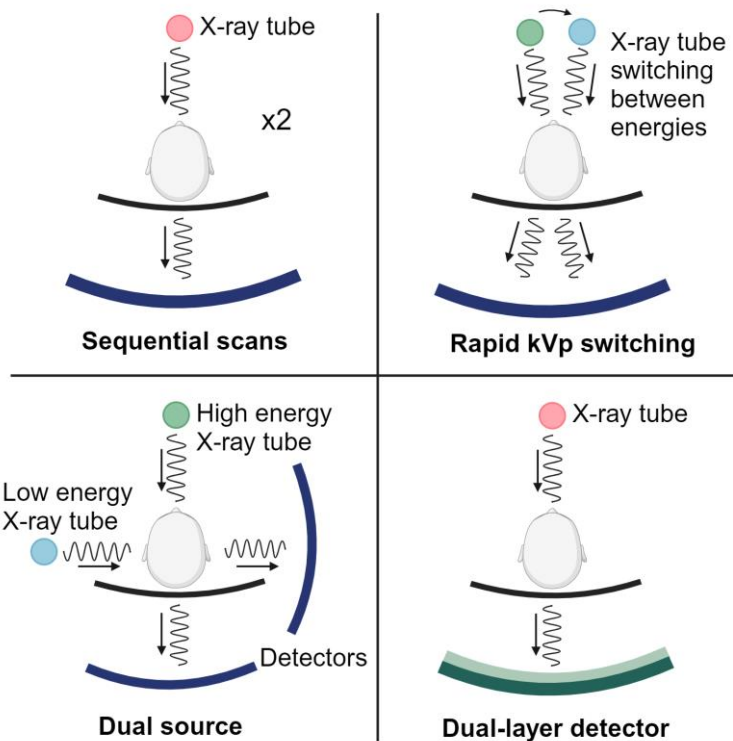


**Figure 6.**

Illustration of different dual energy CT acquisition techniques such as performing two *sequential scans* at different energy levels (top left); single tube and detector system with *rapid kVp-switching* (top right); a *dual source* system with a setup of double, perpendicular, tube and detector systems with different tube energies (bottom left) and a *dual-layer detector* based system which separates the low and high energy data at the detector level (bottom right). Image created in biorender.com

The systems can be grouped into single or double source systems, a full description of all systems is beyond the scope of this thesis but some of the more important systems are described below, and the dual-layer detector technology will be discussed more in depth.

### *Single source systems*

*Sequential scans* performed at different tube energies was one of the first methods to acquire dual energy data and is based on performance of two separate scans at different kVp-levels (usually around 80 and 140 kVp) acquired after one another. This can be performed on basically any CT system but a major drawback is the poor temporal resolution (especially important when performing angiographies). To avoid an increased radiation dose (by two scans) the dose of each scan may be reduced compared to a conventional 120 kVp exam [19, 26].

*Rapid kVp-switching* is also a single source and detector system, this method uses a rapid switch ( $< 1$  ms) [27] between high and low tube energies (eg 80 and 135 kVp) which requires a very rapid alternation between tube potential and, a detector that is able to separate the signals (low signal afterglow). The temporal resolution of this system is good and the full field of view can be used.

The *dual-layer detector* CT (DLCT) has a detector that consists of two separate layers of scintillators detecting low and high energy photons respectively. The outer layer is made of Yttrium and absorbs the low energy photons and the inner layer is made of Gadolinium oxysulfide and absorbs the high energy photons (Figure 7). Light reflectors are placed at the bottom of the detector and the photodiodes are placed in a vertical direction separating different cells of the detector's scintillators (where the reflectors usually are located). The spatiotemporal resolution is excellent, the full field of view can be used and it is possible to create monoenergetic reconstruction in a range from 40 to 200 keV. Also, the material decomposition is performed in the raw data (projection) domain which has, compared to in the image domain, been shown to reduce beam hardening artifacts, this will be further discussed in the section 'Postprocessing' below. Another benefit of this system compared to many of the others, is that it is not necessary to actively choose to scan in dual energy mode, on the contrary, for all scans it is possible to extract and use the dual energy data as well as the combined data for traditional polyenergetic images. Disadvantages include potential data storage considerations since for all exams both spectral information/images and conventional data can be saved.



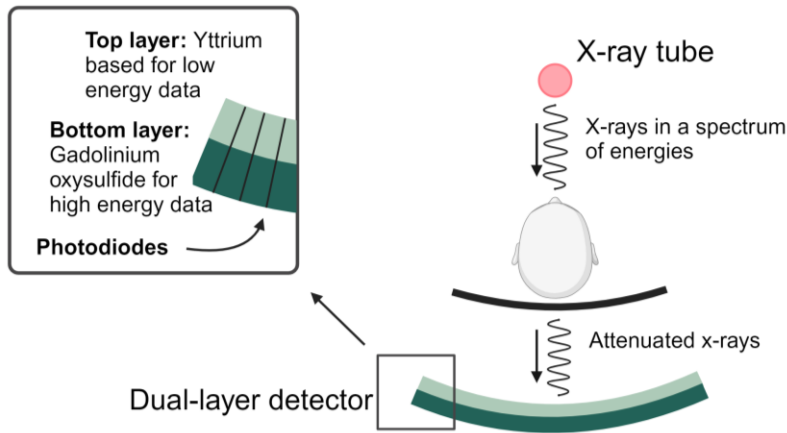


**Figure 7.**

Illustration of the dual-layer detector CT which at the detector level separates high and low energy photons and thus acquires dual energy data. As opposed to a more conventional CT detector, the photodiodes are located in a vertical manner and the light reflectors (not shown) are instead located at the bottom of the outer (high energy) layer. Image created in biorender.com.

### *Dual source system*

The most frequently used dual source system consists of two perpendicular source and detector pairs which simultaneously perform scans at different tube potentials, one in a high energy and one in a low energy. It is possible to independently adjust the settings of each tube and a filter can be used to eliminate the low energy photons from the high energy tubes photon spectrum. However, the high energy detector is usually smaller than the other, due to the limited space in the gantry, which leads to a decreased field of view when performing scans in dual energy mode [19, 26] and there is also the possibility of scatter from the different setups affecting the outcome of the other resulting in a reduced spectral separation [28].

There are variations of the above-described systems and other techniques, for example there is a single source system with a filter at the tube level that generates a *split beam* with one high and one low energy part and, most recently, a system with a *photon counting detector* has become clinically available showing very promising results with high image quality but a low radiation dose. Table 1 summarizes the advantages and disadvantages of the describes system types [18, 19, 24, 26-32].

**Table 1.**

A summary of advantages and disadvantages of four different dual energy CT (DECT) acquisition techniques.

DECT type	Advantages	Disadvantages
<b>Sequential scans</b>	<ul style="list-style-type: none"><li>- Requires no specific hardware</li><li>- Full field of view</li></ul>	<ul style="list-style-type: none"><li>- Poor spatiotemporal resolution may cause artifacts and interfere with material decomposition</li><li>- Prospective DECT-mode</li></ul>
<b>Dual source</b>	<ul style="list-style-type: none"><li>- Tube settings can be set independently</li><li>- Filters on the high energy tube can reduce unnecessary low energy photons from that dataset</li><li>- Two tubes can be beneficial when examining larger patients</li></ul>	<ul style="list-style-type: none"><li>- Scatter between the two source-detector systems may compromise the data</li><li>- Limited field of view</li><li>- Material decomposition in the image domain</li><li>- Prospective DECT</li><li>- Temporal skew between the high and low projections</li></ul>
<b>kVp-switching</b>	<ul style="list-style-type: none"><li>- Good spatiotemporal resolution</li><li>- Material decomposition in the projection domain</li><li>- Full field of view</li></ul>	<ul style="list-style-type: none"><li>- Slightly higher radiation dose compared to traditional single energy CT</li><li>- Prospective DECT</li></ul>
<b>Dual-layer detector</b>	<ul style="list-style-type: none"><li>- Excellent spatiotemporal resolution</li><li>- Material decomposition in projection domain</li><li>- Virtual monoenergetic reconstructions from 40 to 200 keV</li><li>- Full field of view</li><li>- Retrospective DECT</li></ul>	<ul style="list-style-type: none"><li>- Scatter between detector layers may cause energy overlap</li><li>- Data storing considerations regarding saving spectral data from all exams</li></ul>

## Creating the images (postprocessing)

When the CT scan is complete, the data needs to be reconstructed into interpretable images representing the attenuation in all points of the image matrix. The reconstruction process is purely mathematical and rather complicated (at least for non-mathematicians). For many years (decades), only the method of *filtered back projection* (FBP) has been used since it demands less computational power than *iterative reconstruction* (IR). However, since the iterative reconstruction-method enables improved or equivalent (at a lower radiation dose) image quality, IR has received a lot of focus during the last 10 years and is now commonly used in clinical practise. These two mentioned reconstruction methods are described below [21, 33-36].

Reconstruction steps and filters can be performed/applied either in the projection domain (raw data) or in the image domain (after some reconstruction steps are already done, changes are applied to the image data not the raw data).

### The sinogram

The sinogram is produced by applying the Radon transform (a mathematical formula) to the measurement data from the detector's readings. The sinogram represents the digital raw data ('projection data') i.e. the summed attenuation along the path of the x-ray beams (at the different measured angles). The data is stacked along the sinogram in different directions depending on the angle at which the specific data was acquired. After the sinogram is produced the image reconstruction can be performed [21, 37].

### Types of reconstruction

#### *Filtered back projection*

By projecting the data acquired at different angles backwards into a two-dimensional image matrix (applying the same attenuation value to all voxels along the angle), blurred images may be created - this is called back projection. The image is improved with a larger number of projections, but this technique alone does not produce images of sufficient quality, hence, a filter may be applied to the raw data (sinogram data) to reduce the blurring of the images [33].

#### *Iterative reconstruction*

There are two types of IR - hybrid and model-based. The hybrid type is faster (lower computational demands) compared to the model-based type which is more demanding but with even better image quality and/or radiation dose reduction.

There are several available variations of these reconstruction types from different vendors, they usually involve FBP also but with an addition of iterative methods for improvement of the image quality.

*Hybrid iterative reconstruction* combines iterative steps with back projection by first applying iterative filters to the raw data (the sinogram data) to improve image quality, then the back projection is performed after which more iterative filters are applied to improve image quality.

*Model-based iterative reconstruction* is initially based on a back projection to the image domain, the image is then forward projected into projection type data which can be compared to the original raw data and then the pixel values are adjusted accordingly, this process of backward and forward projection is repeated multiple times until the differences are insignificant [21, 37].

## **Filters**

Different additional filters may be applied to the projection data before reconstructing the images. These reduce blurring but also sharpen the image in different ways depending on the type of filter chosen. For example, there are bone filters, lung filters and standard filters (soft tissue). These filters also affect image contrast, noise levels and resolution [21].

## **Reconstructing dual energy images**

As previously described, there are multiple ways to acquire dual energy data, and the reconstruction methods also differs some between the different scan techniques. The foundational difference lay in which domain the reconstructions are made – within the projection (raw data) or the image domain.

Reconstruction within the image domain means that the high and low energy data has already been separately reconstructed into images, and thereafter DECT reconstructions i.e. tissue separation (known as material decomposition, for example iodine maps) can be created. In projection domain-based reconstruction, basis data decomposition is performed using the raw data (creating ‘material raw data’) after which corresponding images can be reconstructed, this enables more DECT applications, for example virtual monoenergetic images (VMIs) can be reconstructed in addition to the material specific images. Reconstructions made within the projection domain are known to demonstrate less beam hardening artefacts) but requires well-matched data sets and is not possible for all DECT systems (See Table 1) [38, 39].

In general, two main types of spectral images can be reconstructed – images based on material decomposition and, ‘virtual monoenergetic’ images.

*Material decomposition* means that the high and low energy data sets (representing predominance by Compton scatter or the photoelectric effect respectively) are compared by creating two data sets corresponding to two elements with different attenuation curves (usually iodine and water) and with these as a 'base' the attenuation curve in each pixel can be compared and characterized. For example, iodine can be characterized and quantified, other examples are calcium (bone) and monosodium urate (crystals that cause gout) [24, 40].

*Virtual monoenergetic images* are reconstructed to correspond to images acquired at a certain monoenergetic level. These can be created by linear combination of Compton and photoelectric data. This can however only be performed if the reconstruction is done in the projection domain. The exact steps of postprocessing are however not generally publicly accessible but kept by the vendors in order to protect their companies' products from competitors.

For the dual-layer detector DECT (IQon, Philips Healthcare, the Netherlands) which is evaluated in this thesis, the postprocessing is performed in the projection space. The high and low energy data can be either combined and reconstructed by model-based or hybrid iterative reconstruction (*IMR* or *iDose*, Philips Healthcare, The Netherlands) into conventional polyenergetic images or the data can be used for a basis decomposition that creates one raw data file for Compton data and one for photoelectric data. Still in the projection domain, spectral reconstruction is performed (Compton and photoelectric images) and saved as an SBI-file (Spectral Base Image-file) in the picture archiving and communication system (PACS). The SBI-file contains all information needed for both material decomposition-images and VMIs and enables retrospective extraction of these different spectral images. See figure 8 for a flow chart of the post processing for the dual-layer detector CT [29, 41, 42].

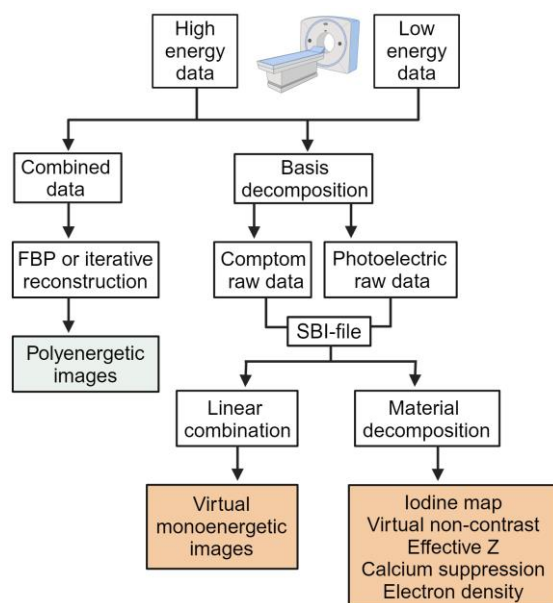


**Figure 8.**

Illustration of the postprocessing of data acquired by the dual-layer detector dual energy CT IQon (Philips Healthcare, The Netherlands). Original figure from *Detector-based spectral CT with a novel dual-layer technology: principles and applications* by Negin Rassouli, Maryam Etesami, Amar Dhanantwari, Prabhakar Rajiah. ©2017 The Authors.

Figure adapted and distributed under the CC BY 4.0 <http://creativecommons.org/licences/by/4.0>.

Adaptations made in biorender.com.

VMIs can be reconstructed in a range from 40 to 200 keV. Through material decomposition several types of images may be created: *virtual non-contrast images* (VNC) where all attenuation by iodine is subtracted from the images; *iodine maps* (either with or without subtraction of calcium (named *Iodine density* and *Iodine no water* respectively) where iodine is visualized and may be quantified; *calcium suppression* where all attenuation by calcium is subtracted from the images; *uric acid* maps for visualization of gout related depositions; *Z effective* images which visualize structures depending on the average atomic number within the tissue and, *electron density* images which display the electron density in a tissue (relative to that of water) [27, 39, 42].

## Image quality

Several factors contribute to the perceived quality of an image, sometimes a high image quality is necessary and sometimes it is more important to keep the radiation dose to a minimum – what is an adequate image quality depends on which questions

that the exam aims to answer. Factors related to image quality are described in this section.

## Image contrast

CT image contrast is the ratio of the attenuation difference between two structures [17]. The contrast makes different tissues and structures distinguishable from one another in the images. Tissue contrast depends on the balance of number of attenuated x-rays (by the photoelectric effect) and the number of x-rays (from the x-ray source) that reach the detector in one tissue related to another. This balance is dependant on the types of tissue and the energy spectrum of the x-rays (and hence the tube potential), with a better low contrast tissue resolution with lower tube potential since in higher kVp a higher proportion of Compton scatter and lower proportion of photoelectric effect will occur. Compton scatter does not contribute to image quality or information but instead raise the overall signal from the tissue which reduces the image contrast and thus Compton scatter is one of the causes of image noise (see below). Aside from altering the tube potential (and using different strategies of noise reduction), the contrast may be increased by administration of a contrast agent (e.g. iodine, barium, water or air). This may alter the attenuation ratio between tissues or areas and hence be beneficial in relation to image contrast [17, 21].

The appearance of image contrast may be changed by altering the window settings i.e. increasing or decreasing the width and level (center) of the presented greyscale.

## Noise

Image noise (called ‘image grain’ by Hounsfield in his 1976 publication on CT image quality) [43] is the small, general variation in a tissue’s attenuation that doesn’t represent any true variation. Many factors contribute to the overall noise; *exam details* (kV, mA, slice thickness, patient size etc); *hardware system* (electronic noise in photodiodes, scattered radiation from the patient) and, type of *reconstruction* (sharper filters adds noise). The balance of noise and other parameters is however not straightforward.

A higher *tube current* increases the number of x-rays generated and therefore increases the number of photons that can contribute to the final image – this leads to a reduced perceived image noise but, results in a higher radiation dose. Similarly, an increased *rotation time* will decrease noise but may increase radiation dose. The tube current and rotation time are sometimes referred to as a product, mAs (mA x s).

An increased *tube potential* increases the proportion of contributing x-rays (it also adds on the number of scattered x-rays but proportionally less so) and thus,

decreases image noise. However, the visualization of low contrast tissues may be impaired (since it depends on a low tube potential) which is a drawback.

Also, increasing the slice thickness reduces the image noise (more photons per slice) but may result in a partial volume effect which reduces the potential of detecting small lesions.

## **Image resolution**

### *Spatial resolution*

The spatial resolution can be described as *detail visualization* – the ability to detect structures that are small or, to separate structures that are close to one another. Spatial resolution depends on many factors, such as detector element size, pixel size (resolution of image matrix, hence resolution is also dependant of field of view (FOV, increased FOV increases pixel size which decreases resolution), pitch (i.e. how ‘close’ the rotations of the spiral are, a higher pitch (wider gaps in the spiral) result in a decreased resolution), focal spot size and, importantly, reconstruction type. As mentioned previously different filters can sharpen the image to increase the spatial resolution, however, these algorithms usually also increase noise values which must be considered [21, 33].

### *Temporal resolution*

Temporal resolution means how well a moving object or tissue is depicted, such as the heart – low temporal resolution equals motion artifacts. The temporal resolution is mainly a measure of how long time it takes to acquire each image slice, this in turn is dependant on the rotation time and the pitch [17, 21].

## **Artifacts**

An image artifact consists of information in the image that does not represent any true structure or irregularity. There are many causes of artifacts, some are due to characteristics of the patient (implants, patient size and positioning) and some represent errors or technical difficulties inherent to CT (such as detector element dysfunction and beam hardening artifacts). *Beam hardening* and *metal artifacts* are common, relevant for the reader of the papers in this thesis and are therefore further described here. Other types of artifacts include aliasing and partial volume artifacts.

### *Beam hardening artifacts*

When x-rays pass through an object the lower energy x-rays are absorbed along the path of the x-ray depending on the material they encounter, the mean energy of the x-rays is therefore increased, and this is usually called ‘hardening’ of the x-rays.



Beam hardening is always present (the beam spectrum is harder the further through the objects that has been passed, this technically results in successively lower attenuation values towards the centre of the scanned object ‘cupping artifacts’) but may be adjusted for before image reconstruction. This kind of successive beam hardening does generally not cause any persistent visible artifacts in the images. However, beam hardening artifacts may become apparent when x-rays pass through a structure with an unusually high density, such as dense bone or contrast agent, which results in dark streaks (‘shadows’), in the tissue on the far side of the high attenuation area (figure 9A).

### *Metal artifacts*

Metal implants may also result in streak artifacts in the images (figure 9B), these are usually caused by a combination of beam hardening and *photon starvation*. Photon starvation occurs when an insufficient number of photons reach the detector to contribute to image data, this results in dark streaks and high noise levels [16, 21, 33, 44, 45].

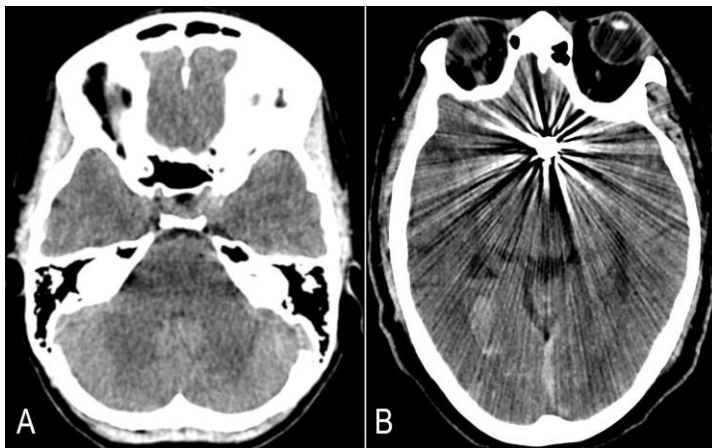


**Figure 9.**

Example images of intracranial beam hardening artifacts in the interpontal pons (A) and metal artifacts by coils (B). The images are derived from the exams of patients that were included in Paper I and IV (Images A and B respectively), figure created by the Author.

## **Measures of image quality**

There are multiple measures, and variations of these measures, used to evaluate image quality in CT. Different measures are used depending on the purpose of the measurement, for example CT scan protocol optimization using phantoms or, evaluation of clinical (patient) images. Measures used for protocol optimization, and comparing the performance of different CT machines are usually performed by CT

physicists and these measures are usually more robust but also more complicated, there are usually also some foundational requirements for the measurements to be performed. Examples of such measurements include *Noise power spectrum* which is a measure of noise levels that (as opposed to the clinically used measures) takes into account the texture of the noise (which may severely affect the appearance of image quality) and, *Modulation transfer function* which is a measure of how well the spatial resolution is kept in the system when the data from the examined object is reconstructed into an image [21, 46].

#### *Standard deviation of attenuation*

The standard deviation (SD) within a measurement of a tissue is a simple indication of the general variation within the measured area i.e. image noise [17, 33, 46].

#### *Signal-to-noise ratio*

The signal-to-noise ratio (SNR) aims to represent the amount of noise in relation to the attenuation values of the examined tissue and can be calculated as

$$SNR=HU/SD$$

where HU represents the mean attenuation in the measured area and SD represents the standard deviation of the measured area. This does not consider the characteristics of the noise, i.e. the noise texture, but is a commonly used approximation of noise in clinical exams (in contrast to image quality assessment studies where phantoms are used). There are variations of the formula for calculation of SNR.

#### *Contrast-to-noise ratio*

The contrast-to-noise ratio (CNR) represents the contrast between two different tissues in relation to the amount of background noise - how well a structure can be delineated. There are several variations in how CNR can be calculated, for example

$$CNR=(HU^1-HU^2)/\sqrt{(SD^1+SD^2)}$$

where 1 and 2 represents the two different examined tissues. The choice of the formula used for calculation of CNR will be further discussed in the *Discussion* part of this thesis.

#### *Posterior fossa artifact index*

The posterior fossa artifact index (PFAI) was first described 1991 in a publication by Roziek et al. where they evaluated different scanning planes in regard to posterior fossa artifacts. The index is based solely on the standard deviation of the HU-value

in a region of interest (ROI) placed posterior to the clivus and represents the severity of beam hardening artifacts in the interpertrous part of pons [47].

#### *Visual grading analysis*

A way to qualitatively evaluate the images by scoring regarding for example noise levels, visualization of different structures and presence of artifacts. This can be done either by comparing one set of images to another (assessing which one is better and, on a scale of for example 5 steps, how similar or different are they) or, by viewing one exam at a time and giving it a score on a predefined rating scale.

#### *Receiver operating characteristics*

Receiver operating characteristics (ROC) analysis are carried out to evaluate the performance of a diagnostic tool or test. Readers are asked to assess whether an assumption is true or false, for example if a specified pathology is present or if a specified structure is visualized in an image. The reader may also be asked to specify, on a scale, how certain they are of this finding or absence of finding. The test is performed using both cases with and without findings in order to determine how many that were accurately assessed as positive or negative and, how many were incorrectly assessed as positive or negative. This data can be presented as a curve where the *area under the curve* (AUC) is a measure of diagnostic accuracy or, measures of test performance, such as sensitivity (how well the true positives are identified) and specificity (how well the true negatives are identified), may be presented [46].

#### *Reader agreement*

The agreement between two readers or between two separate assessments by one reader, can be presented as inter- and intra-reader agreement, respectively. The agreement is often calculated by a Kappa test in which the agreement between readings of the test is compared to the rate of expected agreement by coincidence. The Kappa test provides a number (Kappa coefficient) between -1 and +1, where 0 indicates only coincidental agreement, +1 perfect agreement and, -1 systematic disagreement. Between 0 and +1, the coefficient is often interpreted using a 5-step scale of agreement from Poor agreement to Very good agreement. [46, 48].

## CT in neuroradiology

This section aims to give an overview of parts of the field of neuroradiology, limited to what is relevant in regards to Paper I-IV.

Non-contrast CT (NCCT) of the brain is one of the most common radiological exams in Sweden, in 2018 it came in at the 4<sup>th</sup> place of the most frequently

performed exams of adults (after radiographs of extremities, chest and pelvis). In 2018, close to 355 000 brain NCCT were performed in Sweden, an increase with a little more than 100 000 exams compared to in 2005 [49]. In Region Skåne in Sweden, the price of a plain brain CT is about 1400 SEK and the price of a plain brain MRI about 2400 SEK [50]. If a CT is inconclusive, an additional MRI sometimes is performed to confirm or exclude the suspected diagnosis. Given the amount of brain exams performed, increasing the diagnostic spectrum or accuracy of CT would have an economic value and, more importantly a value for the patients who could receive a diagnosis faster and perhaps not have to go through additional exams or tests.

## Stroke Imaging

When there is suspicion of stroke (intracranial haemorrhage or ischemia), a plain brain CT is performed rapidly, often followed by a perfusion study and CT angiography, especially in case of suspected ischemic stroke.

However, in the hyperacute setting ischemic lesions are difficult to detect since it takes time for the changes in the parenchyma to manifest. The evolvement of visible changes depends on how long time that has elapsed from the occlusion, which vessel that is affected, presence of collateral perfusion to the ischemic area. The detection of lesions also depends on the experience of the CT reader [51].

The first detectable sign is the ‘dense vessel sign’ – in which the clot is visible as an hyperattenuating area within an intracranial artery (typically described in the first segment of the middle cerebral artery). This sign can be detected immediately but is not always present due to the composition of the clot or if the clot is not large enough to be detected. This sign has a high specificity (95%) but a moderate sensitivity (52%) for arterial obstruction [51, 52].

Reduced differentiation of grey and white matter is the first parenchymal sign of ischemia in the under-perfused area, this represents the developing *intracellular* cytotoxic edema (swelling of affected neurons due to cell membrane pump dysfunction (an increased entry of sodium, calcium and water into the cells)). The cytotoxic edema develops in the GM (grey matter) earlier than in the WM (white matter) because the GM has a higher metabolism than WM and is therefore more sensitive to an impaired perfusion [53, 54]. A reduction of grey and white matter contrast can be detected as early as 1 hour after onset (for example in the highly sensitive deep GM nuclei), but in other cases it may take more than 24 hours. The cytotoxic edema is also the cause of another early sign of ischemia - effacement of cortical sulci due to swelling of the affected tissue [55]. Shortly after the cytotoxic edema has started to develop, as the endothelial cells of the blood vessels in the area become affected, a vasogenic, *extracellular*, edema also develops. This edema is caused by a dysfunction in the affected blood vessels (blood brain barrier) resulting

in a leakage of water from the blood to the extracellular space, vasogenic edema is primarily located within the white tissue, causes swelling of the interstitial tissue and appears hypoattenuating and expansive on CT. The cytotoxic and vasogenic edemas cause a progressive expansive effect of variable severity that develops over a period of up to 7 days after onset. This expansive effect includes effacement of sulci, compression of the ventricles and basal cisterns, midline shift and, different types of herniation (Figure 10) [54-57].

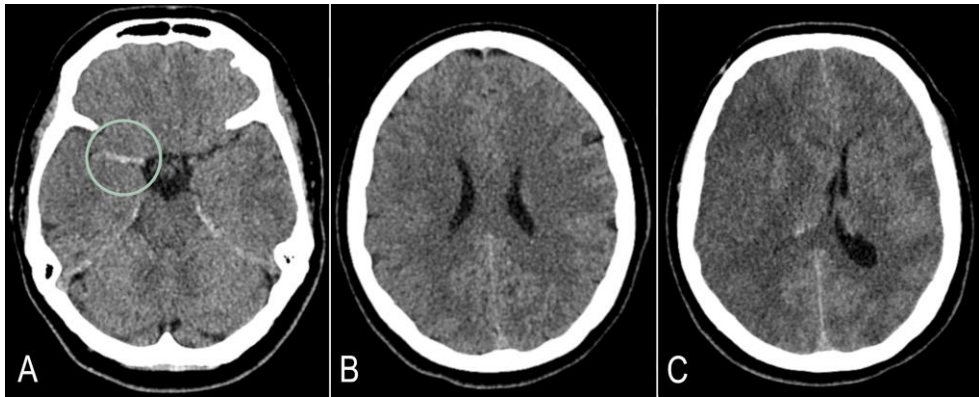


**Figure 10.**

Example of a 'dense vessel sign' in the right M1-segment of the middle cerebral artery (A), reduced grey and white matter differentiation within the territory of the right middle cerebral artery (B) and, progressive edema within the lesion resulting in an expansive effect with effacement of sulci, compression of the right lateral ventricle and, a midline shift to the left (C). A and B images are from the initial exam, performed approximately 2,5 hours after symptom onset, and the exam of image C was performed about 12 hours after symptom onset. The images are derived from the exams of a patient that was included in Paper II, figure created by the Author.

As the swelling starts to subside, a process of cell degradation and recruitment of white blood cells (such as macrophages) occurs in the affected tissue, leading to a temporary increase in tissue attenuation in the ischemic lesion. The lesion can thus become isoattenuating with the non-affected surrounding tissue and thereby difficult to delineate at this point (1-3 weeks after onset), a phenomenon called *fogging* [58-60]. After about 3 weeks, as the dead tissue is resorbed, the affected area turns increasingly hypodense and there is loss of tissue volume including both GM and WM within the lesion [54].

The main purpose of the initial NCCT is to exclude an intracranial haemorrhage, which is a contraindication of administration of intravascular thrombolytic agents (clot dissolvers). However, the extent of visible early signs of ischemia has also been shown to have predictive values of patient outcome, and for this purpose an estimated quantification of the extent of the lesion can be made using for example the ASPECTS (Alberta Stroke Program Early CT Score) or the prASPECTS (posterior circulation Acute Stroke Prognosis Early CT Score) [61-63].

In cases with suspicion of acute stroke and no detected intracranial haemorrhage the plain CT is usually complemented by a following perfusion study and CT angiography. The perfusion study provides an indication of both the presence and the severity of a perfusion deficit, as well as the size of the affected area. Depending on the perfusion deficit, the affected area is typically characterized as either tissue that is not possible to save by reperfusion ('core') and tissue that is potentially salvageable by reperfusion ('penumbra'). This is important for treatment decisions, especially when the time of symptom onset is unknown or when there is a discrepancy between the extent of symptoms and the early signs of ischemia on the non-contrast CT [62, 64].

The CT angiography (CTA) aims to detect the occlusion site as patients with a large vessel occlusion (LVO; occlusions located in the intracranial parts of the internal carotid and vertebral arteries, the first and second segments of the middle cerebral artery, first segments of the anterior and posterior cerebral arteries and, the basilar artery) are less likely to benefit from intravenous thrombolysis but may benefit from endovascular thrombectomy. The CTA can also be used to assess collateral blood flow to the affected area and to assess potential anatomical aspects that may be important for the endovascular procedure such as proximal occlusion or stenosis or vessel tortuosity [62, 65].

If the diagnosis remains unclear, no lesion can be detected on NCCT or the perfusion or angiographic studies, but the suspicion of ischemic stroke remains, a subacute MRI can be performed. Due to the excellent visualization of tissue edema, diffusion weighted MRI sequences have a high (>90 %) sensitivity for acute ischemic lesions [66, 67].

In addition to suspicion/follow up of ischemic lesions there are many other indications for performing NCCT and CTAs of the brain. For example, detection of haemorrhage and/or skull fractures in trauma patients, suspicion of venous sinus thrombosis, evaluation of hydrocephalus, evaluation of severity of tumour related edema etc. All of these have in common that the interpretation of the images may be interfered by image artifacts, why this is common for brain exams is described below.

## **Image artifacts in neuroradiology**

### *Metal artifacts*

As already described, metal causes streak-like artifacts in CT images. There are several examples, both common and less common, of metal implants that can cause artifacts in brain CT. Examples include dental implants, coils or clips used to treat aneurysms and other vascular anomalies, deep brain stimulation electrodes for symptomatic treatment of Parkinsons disease and, fixation material in the skull after

surgery. These implants may all cause severe artifacts in the images and thus interfere with the radiological evaluation of the images [68, 69].

Proper positioning is one way to potentially minimize artifacts from dental implants but artifacts from other types of implants cannot readily be reduced that way. Reducing the artifacts by increasing tube current and voltage is generally not suitable because it would increase the radiation dose. In recent years metal artifact reduction algorithms have been introduced by different CT vendors. These algorithms usually have a name including ‘MAR’ for *metal artifact reduction* and are based on identification of the metal in the projection domain and then, data from unaffected projections is used to calculate a corrected image in an iterative process. These algorithms have been shown to perform differently depending on the type of metal in the implant and have also been found to potentially cause additional image artifacts [45, 70].

Another possible way to reduce the metal artifacts is by using VMIs by dual energy CT. Theoretically, the metal artifacts should be less severe in VMIs in the higher energy levels (that are reconstructed as images acquired by high-energy photons) [45]. This effect, sometimes in combination with MAR algorithms, has been shown for some types of implants.

### *Beam hardening artifacts*

The brain is (thankfully) surrounded by a dense, protective cranium. However, in CT imaging this causes some problems regarding image quality. The cranium absorbs many of the lower energy photons and in especially some locations, such as the posterior fossa, the beam hardening caused by the skull can produce significant artifacts. The posterior fossa is known to be difficult to assess in CT images and in cases with uncertainty an MRI is performed to safely detect or rule out posterior fossa pathology. The petrous parts of the temporal bones often cause a band-like beam hardening artifact through mid-pons. This artifact can be quantified using the previously described PFAI, and potentially these kinds of artifacts may also be reduced in high energy VMIs [71].

## CT contrast medium

Contrast agents have been in use in radiology since at least the 1920’s, then barium and bismuth were used orally for depiction of the gastrointestinal tract [72]. D. F. Cameron was first to describe the use of iodine as a contrast agent and it was rapidly introduced for cysto- and pyelographies thereafter [73]. Soon after the first brain CT was performed in 1971, Dr J. Ambrose noted that intravenous administration of iodine contrast medium (CM) could enhance the visibility of a brain tumor in one of his patients [7, 74].

Currently, the most used contrast medium and administration route in CT is iodine-based contrast used intravenously. In the early 2000s, annual use of about 75 million doses of iodinated CM worldwide was reported. There are unfortunately several disadvantages of iodine-based CM, some of them potentially severe for the individual that receives them, such as anaphylactic reactions and nephrotoxicity [75, 76]. Another disadvantage is the contamination of iodine in the wastewater and potential toxic breakdown products that can affect the eco systems that are exposed. As Dekker et al reported in 2022, iodine CM has been encountered in drinking water in several locations globally [77]. On a day-to-day basis the clinically most discussed disadvantage is probably the risk of inducing acute renal failure, especially in patients with an underlying renal dysfunction.

Contrast-induced nephropathy has been defined as either a 25 % increase of baseline serum creatinine or, in absolute values, an increase of  $\geq 44 \mu\text{mol/L}$  in serum creatinine within 3 days after administration of iodine-based CM after other possible reasons for renal failure have been ruled out [76, 78]. Usually, the renal function impairment is transient, and patients are treated by hydration and a pause in the administration of potentially nephrotoxic medication. However, among patients with risk factors (most importantly chronic renal failure, hypertension and diabetes) up to 30 % may suffer from sustained worsened renal dysfunction [78]. Contrast-induced nephrotoxicity may result in both an increased morbidity for patients and an increased healthcare cost due to medical treatment and prolonged admission time.





# Aims

The overall aim of this PhD-project was to evaluate some of the potential benefits of dual-layer detector dual energy CT in neuroradiology.

Improved image quality or improved diagnostic accuracy in CT exams would be a great benefit for the patients, who may otherwise have to go through additional exams (potentially increasing the radiation dose) or stressful tests, and for the healthcare providers who might be more certain of diagnosis and the following management. With a more certain diagnosis, or exclusion of a diagnosis, comes also the possibility of reduced healthcare costs due to quicker management, less additional or complementary exams (such as MRI) and, shorter duration of in hospital-care. The specific aims of each paper are listed below.

*Paper I.* To evaluate intracranial metal artifacts caused by coils in VMIs compared to in conventional images by a DLCT in non-contrast brain CT images.

*Paper II.* To evaluate whether the ability to detect acute cortical ischemic lesions is improved in DLCT virtual monoenergetic reconstructions compared to conventional polyenergetic images.

*Paper III.* To investigate whether image quality can be preserved in brain CTA with halved CM dose by using VMI reconstructions and to investigate whether VMIs can compensate for poor arterial enhancement.

*Paper IV.* To evaluate posterior fossa artifacts in VMIs by a spectral dual-layer detector CT compared with conventional polyenergetic images from the same exam.



# Materials and methods

All papers in this thesis are single-center, retrospective studies with adult patients. No alterations in patient management or scan protocol have been made for the purpose of these studies.

The exams have been performed using an IQon spectral detector dual energy CT (Figure 11, Philips Healthcare, The Netherlands), scan parameters can be viewed in Table 2.



**Figure 11.**

Image of the IQon spectral CT (Philips Healthcare, The Netherlands) at Skåne University Hospital in Lund. Photo by the Author.

All quantitative measurements have been performed using ISP (IntelliSpace Portal, Philips healthcare, The Netherlands) which is the Philips-developed image post-processing software where VMIs and material specific images may be reconstructed. For all exams, the ROIs were placed at the desired locations in the

conventional polyenergetic images (CIs) of a, for each project, predetermined slice thickness. The values for the virtual monoenergetic series could then be extracted through a spectral diagram for the exact same ROI size and placement as well as the same image slice thickness to ensure comparable measurements. The spectral diagram included data from VMIs at 40 to 200 keV with 10 keV intervals.

In all the Papers, we calculated the *effective dose* for each scan. The effective dose (mSv) serves as an estimate of the risk for long term harm that the radiation generates in the exposed area, it considers that the sensitivity to radiation varies between different types of tissue. The effective dose is calculated by multiplying the Dose Length Product (DLP, mGycm) of the scan (an approximation of the total absorbed dose) with a conversion factor that is specific to different body parts. The conversion factor for brain exams as suggested in the IRCP 103 is 0.0024 mSv/mGycm. The DLP in turn is calculated by the  $CTDI_{vol}$  x the scan length (ie mean output dose per gantry rotation (mGy) x length of the scan (cm)). The effective dose is a commonly used approximation for comparison of radiation doses between different types of exams or for comparison with other exposures, such as the background radiation, but should not be used as a measure of radiation dose for individual patients as it does not consider the patient size [33, 79, 80].

**Table 2.**

Scan protocols for Papers I-IV.

Scan parameter	Paper I	Paper II	Paper III	Paper IV
Tube voltage (kV)	120	120	120	120
Collimation (mm)	64 x 0.625	64 x 0.625	64 x 0.625	64 x 0.625
Rotation time (s)	0.33	0.33	Group 1: 0.5 Group 2: 0.5 Group 3: 0.33	0.33
Pitch	0.359	0.36	Group 1: 0.609 Group 2: 0.609 Group 3: 0.797	0.36

For the qualitative analysis of Paper I-IV we used a software called Viewdex (Viewer for Digital Evaluation of X-ray images) in which you can enter image stacks, questions and answer options for visual grading analysis. The software has been developed at the University of Gothenburg for imaging studies [81, 82]. The software presents the reviewer with the anonymized images of the included exams in a random order. The reviewers can freely scroll through the image stack, adjust window settings and zoom. Using this software, the images can be displayed on diagnostic screens like in the clinical setting, but the reviewers are unable to see any patient or image reconstruction data. At the time of the data collection for Paper I-IV only one image stack per case could be entered and thus only one image plane could be assessed by the reviewers, as opposed to in the clinical setting where at least 3 planes (axial, coronal and sagittal) are commonly used. In the later versions

of the software, however, the possibility of adding several (up to 16) image stacks per case has been added, creating potential for a more clinically accurate and adaptable software [83, 84]. Prior to the image grading in all of the studies, example cases were discussed in a joint session with the reviewers in order to form a consensus on the rating scale.

## Paper I

This was a retrospective observational study and candidates were identified by a consecutive search in our regional PACS database. Patients with intracranial coils and a subsequent NCCT by the IQon scanner and an accessible SBI-file were included. For patients with more than one NCCT by the IQon, only the most recent to the endovascular treatment was chosen. If a patient had been treated with coils in more than one location, the lesion with the largest coil mass was chosen for the artifact evaluation.

The coil skein volumes were calculated as spheres using the largest diameter (measurement acquired in 3D digital subtraction angiography images from the therapeutic intervention) as has been described previously [85].

The quantitative analysis was based on measurements of mean attenuation and the standard deviation within circular ROIs in predefined intracranial locations. The ROI size was standardized to approximately 10 mm in diameter and the size was only adjusted in order to securely avoid a partial volume effect. ROIs were placed in artifact-affected tissue adjacent to and further away from ( $< 2$  and  $\geq 2$  cm respectively) from the coil skein and, reference measurements were made in WM (centrum semiovale) and cerebrospinal fluid (lateral ventricles) without metal artifacts. We chose to include two measurements of artifact affected tissue since the artifacts usually differ in severity depending on the distance from the implant, and we wanted to evaluate if the effect of VMIs also differs with the distance. As described above, the corresponding values of mean attenuation and the standard deviation for each ROI were then acquired for the VMIs through a spectral diagram.

The qualitative analysis was based on a visual grading analysis where two interventional neuroradiologists with  $> 10$  years of experience rated axial images regarding overall image quality, severity of metal artifacts and, grey and white matter differentiation in an artifact free area. Rating was performed using a 5-point Likert scale in the Viewdex software as described above. In paper I we chose to include the CIs and VMIs at 40-80, 120, 140 and 200 keV based on the results of the quantitative analysis which indicated the largest differences between VMI series were to be found in the lower energy levels. The choice of included VMIs was also supported by previous experience and the foundational theory suggesting that the metal artifacts should be less severe in the higher energy levels.

## Paper II

Paper II was a retrospective observational study and candidates were identified by a consecutive search in our regional PACS database. Patients examined on IQon for suspicion of acute stroke with CT examination within 12 h of symptom onset and access to the SBI-file were included if they also had an acute cortical, supratentorial ischemic lesion either on the initial NCCT or on a follow-up NCCT or MRI. The lesion had to be at least 70 mm<sup>2</sup> since we wanted to optimize the chances of retrieving representative measurements (minimize partial volume effect).

For the diagnostic performance analysis, we also included patients where no acute ischemic lesion had been found to serve as negative controls.

For all patients with an ischemic lesion, the location of the occlusion (derived from the CTA report) was noted for ACA, MCA, PCA (anterior, middle and posterior cerebral arteries respectively) and other/unknown (including for example T-type internal carotid artery (ICA) occlusions or when the exact occlusion site had not been established). A measurement was also performed noting the largest diameter of the ischemic lesion on axial reconstructions of either the follow up or the initial exam.

For the quantitative analysis we performed measurements in ischemic grey matter (IGM), normal grey matter (NGM) and normal white matter (NWM). The IGM measurement was drawn as a free shape to include only the GM of the ischemic lesion, if necessary, the placement and shape was carefully guided by the follow-up exam. This ROI was drawn to a size of  $80 \pm 10$  mm<sup>2</sup> which approximately corresponds to the area of a circular ROI of 10 mm in diameter. For NGM and NWM, circular ROIs with a diameter of  $10 \pm 1$  mm were placed in the thalamus and centrum semiovale, respectively, on either side. SNR was calculated for all three ROIs and CNR was calculated for IGM-NWM, NGM-IGM and NGM-NWM using the formulas described in the *Introduction, Measures of image quality*. Differences in attenuation ( $\Delta HU$ ) was calculated for IGM-NWM, NGM-IGM, and NGM-NWM.

The qualitative analysis was performed in two separate parts. First, a visual grading analysis of image quality was performed by two neuroradiologist, both with >5 years' experience, using the Viewdex software. Axial CIs and VMIs at 50, 60 and 70 keV were evaluated regarding overall image quality and the impression of image ability of diagnosing acute ischemia. For the second part, the negative controls were added to the material in order to retrieve measures of diagnostic accuracy. The reviewers were guided by a moderator who provided some clinical information on the patients' symptomatology to create a more accurate (clinical) reading setting. The CIs and VMIs (50-70 keV) were assessed side-by-side, and the reviewers were asked whether there was an acute ischemic lesion, and if so, where the lesion was located and in which image reconstruction the lesion was most clearly identified.

The moderator then determined if the readers had correctly or incorrectly assessed the exam as positive or negative for acute ischemic lesions. For this part one of the readers was a senior interventional neuroradiologist and the other reader a resident in radiology. We chose to include a less experienced reader for this part to possibly demonstrate that the benefit of adding VMIs is not related to experience level but lesion visibility in the images. Patients are admitted with symptoms of acute stroke during all hours and the primary image assessment is often performed by an on-call resident or a radiologist with another subspecialisation than neuroradiology so this is an important factor in image evaluation for acute ischemic lesions.

## Paper III

Paper III was conducted as an evaluation of a clinically initiated protocol optimization aiming to reduce the dose of iodine CM in brain CTA. All adult patients who had a brain CTA by the IQon CT and an accessible SBI-file could be included. Patients with severe metal artifacts in the images, a proximal occlusion in the intracranial arteries or a significant stenosis ( $>70\%$ ) in the ICA on either side were excluded from the analysis.

Three groups with different scan protocols were evaluated; patients in group 1 were examined with our standard brain CTA protocol with a full CM dose, patients in group 2 were examined with a halved CM dose and, patients in group 3 were examined with a halved dose CM and an adjusted scan time for an optimized contrast timing. Protocol 2 and 3 were used over a specific time period and the inclusion of patients for each group was thus based on this. The CM used in the exam was Iomeron 400 mg I/ml (Bracco, Italy), either 60 ml (full dose) or 30 ml (halved dose) intravenously.

The quantitative analysis was based on attenuation measurements within the intracranial arteries, to determine the CM density within the arteries of the brain. Measurements were performed bilaterally in the top of the ICA and the dominant M2 segment of the middle cerebral artery (MCA), in the confluence of sinus and, for reference measurements, in WM superior to the lateral ventricles on either side. For the measurements performed bilaterally (ICA and M2), the mean value was used. CNR was calculated for all vessel measurements in relation to WM and, SNR was calculated as  $HU/\sqrt{SD}$  for all ROIs. As a measure of contrast-timing, a vein-to-artery ratio was calculated for the CIs as  $HU_{\text{confluence of sinuses}}/HU_{\text{mean ICA}}$ .

Axial CIs and VMIs at 50 and 60 keV were assessed regarding image quality using a visual grading analysis performed in Viewdex. Independent grading was performed by four reviewers, one senior interventional neuroradiologist, two radiologists and one consultant stroke neurologist. The reviewers assessed overall image quality, visual representation of the ICA, visual representation of the M2



segments of the MCA and, the timing of the examination. The three first questions were assessed, as in Paper I and II, on a 5-point Likert scale. The fourth question could be assessed as *in an early arterial*, *in a late arterial*, or *in a venous phase*.

## Paper IV

Paper IV was a retrospective observational study and candidates were identified by a search in our regional PACS database. Consecutive patients examined on the IQon CT with NCCT during a predefined period were included if the examination did not show any significant pathology (such as haemorrhage, ischemia or expansivities) and if the SBI-file was available.

Measurements were performed by placement of ROIs in the interpetrous pons, cerebellar WM and GM and in supratentorial WM and GM. The ROI in the interpetrous pons was placed in an image slice with visible artifact streaks through the pons, such artifacts were present in all exams. The cerebellar ROIs were placed in the cerebellar peduncle (WM) on either side and in the cortex in the temporal part of cerebellum (GM). Supratentorially the ROIs were placed in the centrum semiovale (WM) and the thalamus (GM) on either side. All ROIs were circular and drawn to a size of  $10 \pm 1$  mm in diameter. CNR was calculated for GM-WM for both cerebellar and supratentorial GM and WM. SNR was calculated for cerebellar and supratentorial GM and WM as  $HU/SD$  and the standard deviation for the ROI in the interpetrous pons was considered as the posterior fossa artifact index as described in the *Introduction, Measures of image quality*. The difference in mean attenuation ( $\Delta HU$ ) between cerebellar WM and the attenuation in the interpetrous pons was calculated as  $HU_{\text{cerebellarWM}} - HU_{\text{interpetrous pons}}$ .

A qualitative analysis was performed, two reviewers independently assessed axial CIs and VMIs at 40-80, 100, 120, 140 and 200 keV using Viewdex software. The selected VMIs were chosen based on previous experience and visual assessment of graphs of the quantitative data. A total of 40 of the included 188 patients were also included in the qualitative analysis. The reason to not include all cases was based on the assessment that this would be a large enough population and to reduce the time-consuming task of grading since 13 different reconstructions per patient were evaluated. One of the reviewers rated all exams twice to retrieve data for calculation of intra-reader agreement. Reviewers were asked to assess overall image quality, grey and white matter differentiation in the temporal part of cerebellum and supratentorially and, artifact severity in the interpetrous pons, temporal part of cerebellum and supratentorially adjacent to the cranium (just below the vertex) on a 5-point Likert scale. The reviewers were also asked to decide whether it was possible or not to rule out major pathology in the cerebellum and pons and,

supratentorially. The phrase ‘major pathology’ was suggested to indicate significant haemorrhage or a large ischemic lesion.

## Statistical analysis

For all papers, the statistics used have been discussed with professional statisticians during the study design, and again prior to the analysis. All analyses have been carried out by one or more of the authors. For papers I, II and IV the IBM SPSS (IBM Corp, Armonk, New York, USA) versions 25 (paper I and II) and 28 (paper IV) and MedCalc software (MedCalc Software, Ostend, Belgium) version 20.009 (paper I), 19.3.1 (paper II) and 22.023 (paper IV) were used. MedCalc was used to calculate inter- and intra-reader agreement in Paper I, II and IV and, in Paper II it was used for the analysis of diagnostic capacity (the second part of the qualitative analysis). For the analysis of diagnostic capacity, a 2x2 table was created in which all cases (study subjects and the negative controls) were defined as true positive or negative, or, false positive or negative after which the analysis of diagnostic capacity was performed in MedCalc.

For paper III the statistical analyses were performed using RStudio version 1.3.1093 (RStudio Team, Boston, USA) and VGC Analyzer v. 1.0.3 (University of Gothenburg, Gothenburg, Sweden) [86-89].

Depending on the number of included patients and visual assessment of the distribution of the data, parametric or non-parametric statistical tests have been performed. A p-value <0.05 was considered significant.

## Ethical considerations

All papers included in this thesis were conducted following the Helsinki Declaration and approved by the Swedish Ethical Review Authority (reference number 2019-02225) and informed consent was waived by the Ethical Review Authority.

All of the studies are retrospective and based on collection of patient and image data (which then was anonymized) and visual grading of anonymized images. No additional exams or clinical follow-ups were performed and so the patients were not exposed to any additional radiation or stress of any kind. The protocol changes that enabled Paper III were introduced as a clinical optimization project which we then evaluated.



# Results

The number of included patients and basic patient characteristics for Papers I-IV have been summarized in Table 3.

**Table 3.**

Summary of characteristics of the included patients and the effective doses of exams.

	Paper I	Paper II	Paper III	Paper IV
Number of included patients, n	32	29 (and 23 negative controls)	Group 1: 52 Group 2: 29 Group 3: 43	188
Sex; male/female, n	13/19	20/9 (12/11)	Group 1: 30/22 Group 2: 13/11 Group 3: 16/23	77/111
Median age, years (Interquartile range)	59 (49-72)	67 (62-81)	Group 1: 68 (57-75) Group 2: 75 (52-78) Group 3: 72 (57-79)	68 (45-79)
Median effective dose, mSv (Interquartile range)	2.0 (1.8-2.1)	2.0 (1.8-2.1)	Group 1: 2.5 (2.0-3.2) Group 2: 2.5 (1.8-2.8) Group 3: 2.7 (2.3-3.5)	1.8 (1.7-2.0)

## Paper I

A total of 32 patients were included. The most common coil location was within aneurysms in the anterior communicating artery (n=16) and the median coil skein volume (IQR) for all locations was 93 (34-296) mm<sup>3</sup>.

In the quantitative analysis, the attenuation values of the ROIs in distal artifact, artifact free WM and CSF showed similar patterns with decreasing HU values with increasing energy levels. The measurement in artifact affected tissue close to the metal implant did not demonstrate the same pattern. The attenuation values of the ROI placed in a distal part of the artifacts were significantly higher in VMIs at 50 and 60 keV compared to in CIs. No significant difference was detected between CIs and VMIs for artifact affected tissue close to the metal (Figure 12).

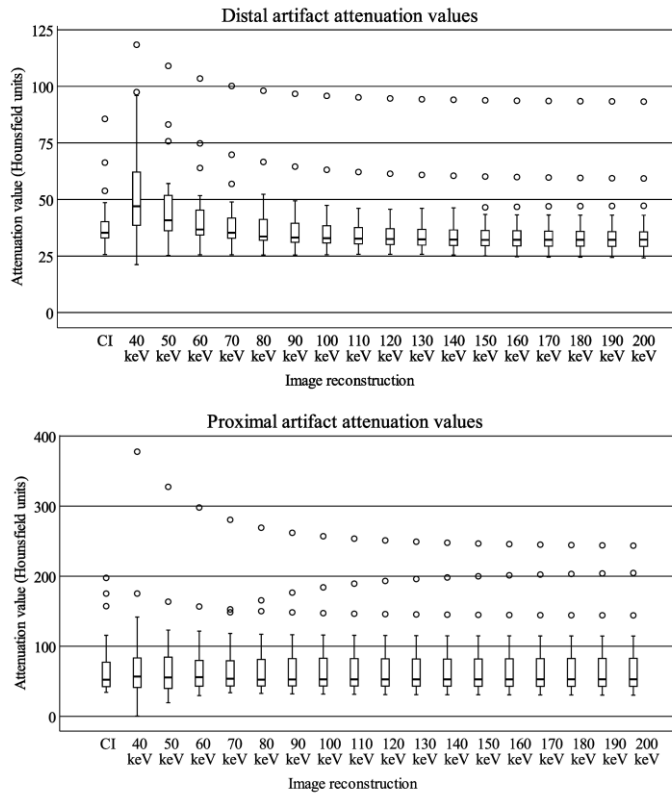


**Figure 12.**

Box plots of attenuation values measured in artifact affected areas at  $< 2$  (proximal) and  $\geq 2$  cm (distal) from the coils respectively. Figure modified from Paper I and redistributed under the CC BY 4.0 <http://creativecommons.org/licenses/by/4.0>.

In the visual assessment of the image reconstructions the 50 and 60 keV reconstruction received the best scores for overall image quality (tied for 50 and 60 keV for reviewer 1 and, for reviewer 2 the 60 keV VMIs received the highest score), significantly higher than the scores of CIs for both reviewers. For this analysis the inter-reader agreement was fair.

For grey and white matter differentiation, VMIs at 50-70 keV all received significantly higher scores than CIs with a moderate inter-reader agreement.

Regarding artifact severity the scores for 50 keV VMIs were significantly higher than for CIs for reviewer 1 but generally the differences in scores were small and no significant difference between CIs and VMIs was found for reviewer 2. The inter-reader agreement was moderate.

## Paper II

We included 29 patients with a confirmed acute, cortical ischemic lesion and, 23 control subjects. The majority of the occlusions were located in the MCA (66 % of all). The median value of the maximum lesion diameter in axial images was 3 cm.

We found generally higher SNR values in VMIs for both ischemic and normal GM and for WM compared to CIs. In normal (i.e. non-ischemic) parenchyma, the CNR between normal GM and WM was significantly higher in VMIs at 40-70 keV compared to in CIs. CNR for NGM-IGM was significantly lower in VMIs at 40-60 keV compared to CIs and in IGM-NWM the CNR was significantly higher compared to CIs in VMIs at 40-70 keV. See Figure 13 for example images from one of the patients.

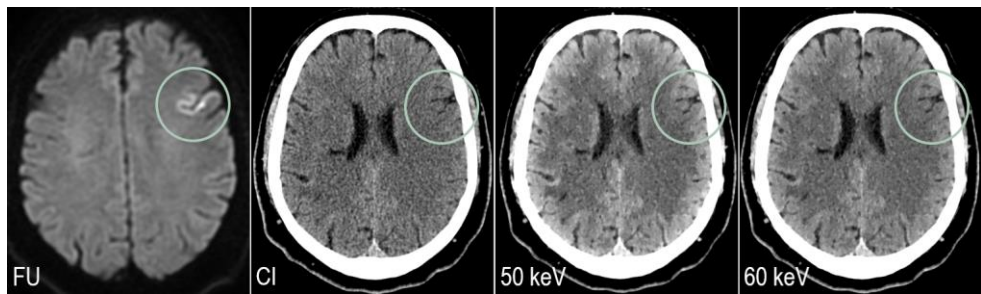


**Figure 13.**

Example case illustrating an ischemic lesion in a DWI-sequence from a follow-up (FU) MRI performed the day after symptom debut in a patient with a small, cortical ischemic lesion in the left frontal lobe. Conventional polyenergetic images (CI) and monoenergetic reconstructions at 50 and 60 keV from the initial CT are also displayed. The images are derived from the exams of a patient that was included in Paper II, figure created by the Author.

VMIs at 50-60 and at 60 keV (for each of the two reviewers respectively) received the highest scores for Overall image quality, all VMI-levels received higher scores than CIs with a moderate agreement between the reviewers. The 50 and 60 keV reconstruction received the highest score for Impression of image ability of diagnosing acute ischemia for reviewer 1 and 2 respectively (also with a moderate agreement). The evaluation of diagnostic capacity showed an improved sensitivity for detection of acute ischemic lesions when assessing a set of images including CIs and VMIs at 50-70 keV compared to assessment of CIs alone (as per the original report). The specificity was lower for both reviewers compared to the specificity of the original report. The agreement between the two reviewers was very good. The diagnostic measures can be found in Table 4.

**Table 4.**

Diagnostic performance with 95 % confidence intervals for detection of acute, cortical ischemic lesions in CIs only (original report) or with CIs in combination with VMIs at 50-70 keV (reviewers 1 and 2). Table modified from Paper II and redistributed under the CC BY-NC 4.0 <http://creativecommons.org/licenses/by-nc/4.0>.

	Original report	Reviewer 1	Reviewer 2
Sensitivity	0.55 (0.36-0.74)	0.93 (0.77-0.99)	0.97 (0.82-0.99)
Specificity	1.0 (0.85-1.0)	0.82 (0.61-0.95)	0.91 (0.72-0.99)
NPV	0.64 (0.54-0.73)	0.90 (0.71-0.97)	0.95 (0.75-0.99)
PPV	1.0 (n/a)	0.87 (0.73-0.94)	0.93 (0.79-0.98)

## Paper III

In the full CM dose group 52 patients were included (group 1), in the group with a halved CM dose and suboptimal timing 24 patients were included (group 2) and, in the group of patients who received a halved CM dose with optimized timing (group 3) 39 patients were included.

For all three groups and all reconstructions the attenuation values of ICA, M2 and the confluence of sinuses peaked in group 1. Comparing groups 2 and 3, the attenuation values in the confluence of sinuses were higher in all reconstructions for group 2 compared to group 3 and the arterial attenuation values in all reconstructions were higher in group 3 compared to group 2.

The CNR for ICA and M2 in group 3 were significantly higher in VMIs at 40-60 and 40-50 keV, respectively, compared to the CNRs of the same locations in CIs of group 1 (Figure 14). Between the groups with halved CM dose, the CNR in ICA and M2 was significantly higher in VMIs at 40-50 keV in group 2 compared to the CNR of the CIs of group 3.

In the qualitative analysis, VMIs at 50 keV had the best ratings for Overall image quality, and the best scores for Visual representation of both ICA and M2, within each group. The 50 keV VMIs of group 3 received significantly higher rating scores for all aspects than the CIs of group 1. The VMIs of group 2 did not receive significantly lower scores than the CIs of group 1. There was no detected difference in vein-to-artery ratio between group 1 and 3.

The inter-reader agreement was moderate to very good.

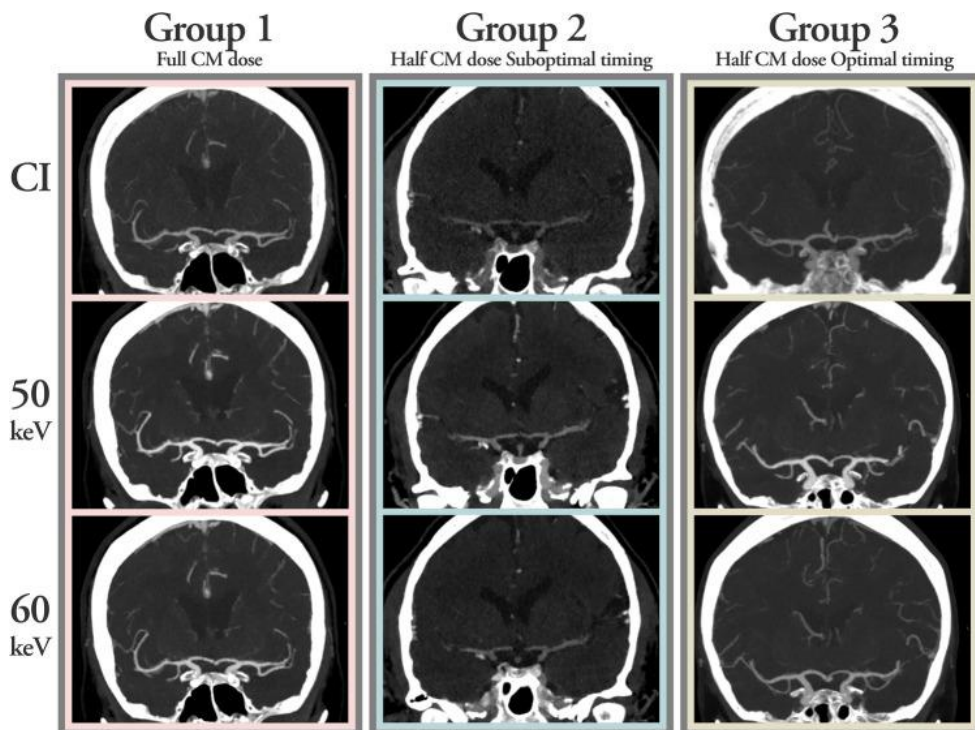


**Figure 14.** CTA example images from all three groups, conventional polyenergetic images (CI), and monoenergetic reconstructions at 50 and 60 keV are shown. CM: contrast medium. Figure redistributed from Paper III under the CC BY 4.0 <http://creativecommons.org/licenses/by/4.0>.

## Paper IV

We included a total of 188 patients in the quantitative analysis and found that the PFAI was significantly lower (lower values indicating less artifacts) in VMIs  $\geq 50$  keV compared to in CIs. Also, the SNR values in the posterior fossa (and supratentorially) was significantly higher in VMIs  $\geq 50$  keV compared to CIs. For both supra- and infratentorial matter the CNR was at its highest in the 40 keV VMIs and was significantly higher than in CIs in reconstructions at 40-80 keV. The  $\Delta$ HU between cerebellar WM and the mid-pons measurement showed the largest difference in CIs and a generally decreasing difference in reconstructions from 40 to 200 keV (significantly lower in all VMIs compared to CIs).

In the qualitative part, patients 1-40 were included and the results correspond well to the results of the quantitative part. For Overall image quality, VMIs at 50-80 keV received significantly higher scores than CIs for both reviewers. The grey and white



matter differentiation, both infra- and supratentorially, was better in VMIs at 40-70 keV than in CIs.

In the assessment of artifact severity in mid-pons, the VMIs at 60 and 100 received the best scores for reviewer 1 and 2 respectively. VMIs  $\geq 60$  keV received significantly better scores than CIs for both reviewers, see Figure 15 for an example. In the temporal part of cerebellum, the 60 and 200 keV reconstructions received the best scores for reviewer 1 and 2 respectively, the score was significantly better compared to the score of CIs for reviewer 1 but not for reviewer 2.

In the evaluation of ability to exclude major infratentorial pathology, VMIs at 60 and 70 keV had the lowest proportion of non-diagnostic exams for reviewer 1 and, for reviewer 2 the 70 keV reconstructions had the lowest proportion of non-diagnostic exams.

The inter-reader agreement was fair for Overall image quality and for Artifact severity in the temporal part of the cerebellum. The intra-reader agreement (reviewer 1) was moderate for Overall image quality but poor for Artifact severity in the temporal part of cerebellum.

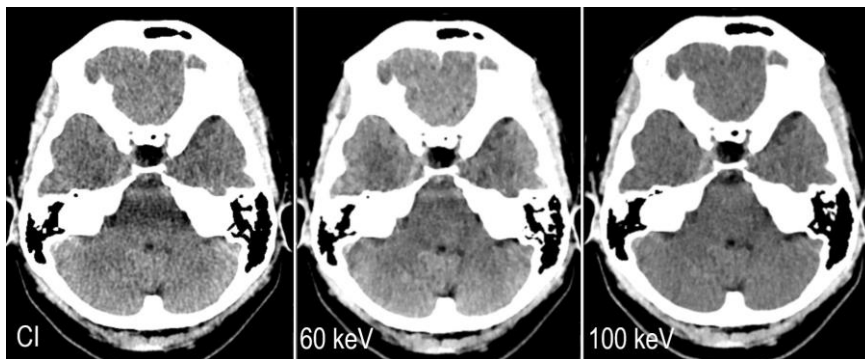


**Figure 15.**

Example images illustrating the severity of artifacts in the interpetrous pons in a conventional polyenergetic image (CI) and in virtual monoenergetic images at 60 and 100 keV respectively. Images are derived from the exam of one of the patients included in Paper IV, figure by the Author.

# Discussion

## What are conventional images?

The term ‘conventional’ could be considered as rather debatable since CT, and diagnostic imaging in general, is constantly evolving. For Paper I-IV, we have used the term ‘conventional’ as a synonym to ‘polyenergetic’. That is, the images are conventional in the sense that they represent the attenuation of photons of a spectrum of different energies, as opposed to the monoenergetic images that are representing images acquired using a specific energy level of the photons.

There are however some considerations that one should reflect upon and one of them is how the images have been reconstructed. In Papers I-IV, the ‘conventional’ images have been reconstructed with an iterative reconstruction technique named *iDose* (Philips Healthcare, The Netherlands), which is a hybrid iterative reconstruction algorithm that was introduced in the early 2010s [37, 90]. As described in the Introduction there are several different ways to reconstruct CT images, and the CT manufacturers have typically developed their own algorithms (such as *iDose* from Philips (Philips Healthcare, The Netherlands) that may differ in the appearance of the final images, and it may also be possible to set the ‘strength’ of the iterative noise and artifact reduction using different levels of the algorithm in the post-processing.

In that sense, conventional images are not necessarily equal and, comparisons between different vendors are further complicated by the intricate interplay of other factors affecting image quality (radiation dose, detector element size, resolution of the image matrix, kernels) [91, 92]. In Papers I-IV however the same IR-reconstruction type and level has been used for both the poly- and monoenergetic reconstructions, which are acquired by the same machine with the exact same scan parameters, so the detected differences in image parameters are not a result of different reconstruction choices, except for the differences inherent to poly- and monoenergetic images.

## Exam radiation doses

Smith-Bindeman et al. performed a prospective, international multicenter study, that included over 600 000 head CT exams and reported effective doses of 1.4-1.9 mSv for brain exams [93]. Those doses represent studies performed in different countries and with different hardware (machines from four major manufacturers were represented) and the doses are comparable to the effective doses of Paper I, II and IV (median effective doses of 2 for Paper I and II, and 1,8 for Paper IV). Thus, dual-layer detector brain CT does not seem to induce an increase in effective doses. The median effective doses of the three groups in Paper III ranged from 2,5 to 2,7 mSv. A higher dose (compared to Papers I, II and IV) was however to be expected since many of the exams in paper III also included the neck (from the aortic arch) and thus the scan length was generally greater in the CTA-project.

## Evaluation of image quality

### Quantitative measures

Evaluation of the quality of clinical CT exams is not entirely straightforward. As described, there are several different measures that can be used and variations of them. For example, the calculation of noise (and in turn the calculation of SNR and CNR) can be performed differently. In Papers II and IV the SNR was calculated as  $HU/SD$  but for Paper III it was calculated as  $HU/\sqrt{SD}$ . For CNR, the noise can be estimated as the sum of the standard deviations of the adjacent tissues, the square root of the sum of standard deviations, the square root of the sum of the squared standard deviations or, the standard deviation of the background tissue. For CNR calculation in Paper II-IV, we chose the calculation of noise as a combination of the SD for tissue 1 and 2 since noise levels might differ between tissue types and thus both be of importance for distinguishing between the tissues. In Paper III we chose  $\sqrt{(SD_1^2 + SD_2^2)}$  formula since it mathematically is an appropriate way to sum standard deviations, however, for Papers II and IV we chose the  $\sqrt{(SD_1 + SD_2)}$  formula, since it was the most commonly used formula in studies that we wanted to compare our results with and we considered the most important factor was that we used the same formula for both the CIs and VMIs [94-97].

Another challenge in image quality evaluation is that there is no standardized way to quantitatively measure metal artifacts. In Paper I we chose to evaluate the artifacts using circular ROIs both near and further away from the metal implant. The artifacts caused by coils are, however, generally alternating hypo- and hyper-attenuating, as opposed to some other types of metal implants, for example clips or hip replacement implants, which can cause a more overall hypoattenuating streak. Using ROI-

measurements to acquire the mean attenuation value of the included area could be problematic for measurement of artifacts that are alternating hypo- and hyper attenuating such as for coils. Other attempts have been made to measure the alternating streaks separately or measuring the minimum and maximum values within an area, the methods differ between studies which complicates comparison of results between studies [69, 98, 99]. In many studies, VMIs for metal artifact reduction has been evaluated along with evaluation of iterative metal artifact reduction algorithms (MARs), usually both separately and in combination (MAR applied to VMIs), and it generally seems that the greatest metal artifact reduction is generated by the MAR-algorithm in combination with VMIs [69, 98, 100-102]. The differences between different metal implants have to be considered when evaluating the effect of metal artifact reduction since implants vary largely in size, shape and in which metal that is used (different atomic numbers). These factors affect the type of artifacts that the implant generates (variations in the proportions of photon starvation and beam hardening) and can affect how well the methods of metal artifact reduction perform (VMIs and MARs respectively) [45]. A robust method for quantitative evaluation of metal artifacts, regardless of type of implant, would be a welcome tool for future studies.

## **Qualitative measures**

When evaluating new clinical tools qualitatively and comparing them to the standard procedure used in the clinic there is a potential risk of a bias towards the standard procedure. That is, since the rater is accustomed to how the reference appears or should be interpreted, they could possibly lean towards applying better scores on the reference procedure. For some of the analyses of Papers I-IV it is also important to point out that some of the VMIs, such as the extremities at 40 and 200 keV, are quite distinguishable (even though no reconstruction data was shown) to the reviewers. For those VMIs the reviewers might have suspected which reconstruction they were rating, possibly resulting in an under- or overrating of those images.

Another difficulty in qualitative analysis with several reviewers is that the steps of the rating scale should have the same significance for the reviewers, also, the questions need to be expressed in a manner that reduce the risk of discrepancy in the interpretation. An important distinction is whether an exam is diagnostic or not, this can however depend on what type of pathology you aim to exclude or detect. For example, in Paper IV there was a rather large discrepancy between the reviewers regarding ‘the possibility to rule out major pathology in the posterior fossa’ where 10 and 63 % of the CIs were assessed as of insufficient image quality to rule out major pathology by the two reviewers respectively. In all of the projects, joint sessions were held with the reviewers prior to the rating session, in order to discuss and exemplify the questions and the rating options. We did not, however, use a

written definition of the steps of the scale as some evaluations are difficult to summarize (such as impression of overall image quality) or could affect the images differently from case-to-case (for example the extension and intensity of artifact).

We chose a 5-point Likert scale since we thought that 5 steps would provide meaningful differences in image quality between individual steps, yet still find small, but potentially relevant differences. Also, several previous studies evaluating CT image quality have used a 5-point scale [97, 103-105].

Since both qualitative and quantitative measures of image quality have their potential limitations, we considered it only more important to perform both types of analysis in Papers I-IV, and to interpret the results jointly.

## CT angiography

In CT angiography the intravascular contrast attenuation and the timing of the study are important factors for the quality of the exam. For some patients, we are faced with the decision between lowering the dose of CM, at the risk of performing a suboptimal exam, or, administering the ordinary dose at the risk of contrast-induced nephropathy. Patient size is usually also a factor in that decision.

For acute brain CTA, and several other angiographic exams with suspicion of fatal conditions, the risk of nephropathy is usually disregarded because of the importance of a correct diagnosis in the acute setting, an inconclusive exam cannot be risked.

In paper III however, the results clearly demonstrate that the risk of an inconclusive exam using a significantly lowered CM dose with low-energy VMIs is small, on the contrary, an improved arterial attenuation could be acquired. These results are in line with results of other studies evaluating other types of angiographies, such as aortic exams, exams for evaluation of pulmonary embolism and abdominal exams for evaluation of malignancy [105-109].

Also, CM is not only used in angiographies but in contrast-enhanced exams in general such as in evaluation of parenchymal organs, enhancement patterns for characterization of focal lesions, for evaluation of ureteral obstruction and, in endovascular procedures. Iodinated CM is one of the most prescribed pharmaceuticals worldwide [110] and methods of decreasing the amount of iodinated CM have been discussed, particularly during the shortage of iodinated CM in 2022 due to the Covid-19 pandemic when the use of dual energy CT was suggested as one of the methods to decrease the use of iodinated CM [111].

Reduction of the use of iodinated CM is beneficial not only for our patients, but for the environment because of the known wastewater contamination of iodine CM and,

is important for a better resilience to potential shortage of this extensively used pharmaceutical.

## The use of VMIs

It seems that there is not *one* optimal energy level VMI, instead, the use of VMIs could be approached as different sequences of MRI, or like adjusting the window settings, and radiologists could independently choose which VMI they prefer for certain evaluations. For example, VMIs at 50 keV could be used for assessment of angiographies, the 50 or 60 keV VMIs for assessment of ischemia and, VMIs  $\geq 60$  for assessment of the posterior fossa. Perhaps not feasible at all times during on call-hours, when the time for assessment of each exam is limited. However, with VMIs becoming more common in the clinical routine, even less experienced readers could become acquainted with VMIs during office hours and time could be saved when they are on call since they know how to use the VMIs for certain tasks, such as evaluating posterior fossa pathology or in CTAs with poor arterial enhancement.

Apart from what has been evaluated in this thesis, as mentioned in the Introduction, there are several interesting features of dual-layer detector CT. For example, the virtual non-contrast images have been shown to be beneficial for the differentiation between hemorrhage and contrast leakage after endovascular thrombectomy [112, 113] or as an adequate replacement of the true NCCT that often is performed prior to a contrast enhanced study or an angiography [114-117]. Also, the iodine maps, which display and allow quantification of iodine have been evaluated for detection of acute ischemic lesions in multiphase brain CTA, evaluation of pulmonary perfusion for suspicion of pulmonary embolism and can be used as an aid in detection of malignant melanoma metastases [118-120].

## Strengths and limitations

One of the main strengths of these projects is the fact that both quantitative and qualitative measures have been evaluated, this enhances the interpretability of the results, especially when the results are coherent, but also when they are not. A limitation that is present for all of Papers I-IV is that the method (both hardware and software) evaluated is vendor-specific and thus not generally available or possible to attain. Another limitation for Papers I-IV is the fact that only axial images were included in the qualitative analysis since we chose to use the Viewdex software which, at the time, only allowed viewing of one image plane per case. Although radiologists, in my experience, generally are fond of axial images, this method does not correspond to clinical routine where usually all three image planes are assessed

and multiplanar reconstruction (MPR) can be used to freely visualize different angles/planes when needed. This may have had both a positive and a negative effect on scores for all reconstructions but, importantly, both CIs and VMIs were evaluated under the same conditions.

In Paper II we also included an analysis of diagnostic performance assessing both positive and negative cases for presence of acute ischemic lesion, this is an important strength of Paper II since it provides further evidence that VMIs increase the detectability of ischemic lesions. As importantly is the fact that VMIs of exams with suboptimal CM timing were assessed in Paper III, the finding that the use of VMIs can reduce the number of non-diagnostic exams is equally important as the results demonstrating a superior image quality in VMIs using a reduced CM dose compared to polyenergetic images with a full CM dose.

## Clinical impact

With the increasing knowledge of the potential advantages of VMIs (and other DECT applications) by dual-layer CT in recent years, at the Department of Radiology in Lund, the protocols used in daily routine have been adjusted. VMIs have gained a more central role, and in exams performed by the IQon spectral CT, VMIs at 50 keV are now standard reconstructions in both brain NCCT and CTA exams. Also, VNC reconstructions have been added in the protocol for NCCT exams performed following endovascular thrombectomy in order to differentiate between haemorrhage and contrast extravasation.

# Conclusions

In conclusion, in all of Papers I-IV, VMIs by dual-layer detector CT generally received better scores for overall image quality compared to the conventional polyenergetic images from the same exam. The VMIs have also been shown to increase the diagnostic potential for early ischemic lesions, decrease artifacts and enhance the quality of CT angiographies so that a reduced CM dose can be administered, or a poor contrast timing can be compensated for.

VMIs by dual-layer detector CT can be a valuable tool and should be used, at least as a complement to polyenergetic images, in the clinical day-to-day routine.





# Moving forward

It would be interesting to evaluate the performance of VNC images by dual-layer detector brain CT, both for contrast-enhanced exams (parenchymal) and, for both arterial and venous angiographies. If the VNC images could replace the true non-contrast series, radiation would be saved, especially important for young patients (for example evaluation of sinus thrombosis in young women) and for patients that are followed regularly with brain CT (such as metastasis screening in cancer patients).

There is also a need for further studies on the diagnostic performance of DECT images, for example, does the improved image quality in VMIs actually increase the diagnostic accuracy of posterior fossa pathology.

Currently, photon-counting CT is extensively evaluated, it enables measurement of the energies of each photon that hits the detector, and therefore provides very precise spectral information. The detector is made up out of one single element, so the actual detector area is not decreased by the spaces between the separate elements (reflector or photodiode columns) in current detectors. More acquired information per photon enables increased image quality and/or decreased radiation dose per exam, these are the main benefits of photon-counting CT [121].

Also, there is continuous development in image reconstruction, where new techniques using deep learning AI are being developed and evaluated in comparison to current iterative reconstruction methods [122].



# Acknowledgements

This thesis is really a result of the work and collaboration of many, without whom this thesis would not have been conceivable.

I would like to express my utmost gratitude to my supervisors for giving me the opportunity to become a researcher! My main supervisor, Johan Wassélius, has been present and encouraging at all times. And my co-supervisors, thank you Birgitta Ramgren for your exquisite attention to detail in proof-reading and your advice in many decisions on methodology, Teresa Ullberg for sharing your knowledge and experience to make these projects clinically relevant and, Kristina Ydström for your guidance in the world of CT physics. Thank you all.

I would also like to deeply thank Veronica Fransson, my dual energy PhD-comrade, for all of your collaboration, thoughts and physics-related help.

Amir Hilal, thank you for your help in Paper II and for your presence and little peptalks along the way.

Björn Hansen for your work in Paper IV (especially thanks for rating all those exams...) and for your support in the final stages of the work of this thesis.

Thank you Per Undrén, Henrik Andersson, Mattias Drake and Francesco Arena for your help as qualitative raters, I know it was time-consuming.

Pär Bengtsson, thank you for allowing me to continue the work that resulted in Paper II.

Thank you, Jimmy Lätt, for your contributions to Papers I and II.

Thank you Region Skåne for funding much of the work that resulted in this thesis. Thank you Peter Hochbergs, Head of the Department of Medical imaging and Physiology at Skåne University Hospital, Gylfi Asbjörnsson and Håkan Sjunnesson, past and present Head of residents in radiology (including me) at Skåne University Hospital and thank you to all of my colleagues who have allowed me the time to work on these projects.

Thank you to the members of and administrators at the Faculty of Medicine at Lund University, especially Ulrika Andersson.

Lee Nolan for attentive and thorough language editing of Papers I-IV.

David Fällmar and Pontus Timberg for your input as opponents at the half-time review.

Gregor Pahn and Matthijs Kruis at Philips Healthcare for your help, especially in the beginning of this project.

My loving and supportive parents, Marianne and Gunnar. My best friends and sisters, Erika and Maria. To Carl and Silje. I'm lucky to have you <3.

# References

1. Cormack AM. Representation of a Function by Its Line Integrals, with Some Radiological Applications. *Journal of Applied Physics*. 1963;34:2722-2727.
2. Cormack AM. Representation of a Function by Its Line Integrals, with Some Radiological Applications. II. *Journal of Applied Physics*. 1964;35:2908-2913.
3. McCollough CH, Rajiah PS. Milestones in CT: Past, Present, and Future. *Radiology*. 2023;309:e230803.
4. Schulz RA, Stein JA, Pelc NJ. How CT happened: the early development of medical computed tomography. *J Med Imaging (Bellingham)*. 2021;8:052110.
5. Hounsfield GN. Computerized transverse axial scanning (tomography). 1. Description of system. *Br. J. Radiol*. 1973;46:1016-1022.
6. Ambrose J. You Never Know What is Just around the Next Corner. *Rivista di Neuroradiologia*. 1996;9:399-404.
7. Beckmann EC. CT scanning the early days. *Br. J. Radiol*. 2006;79:5-8.
8. Bhattacharyya KB. Godfrey Newbold Hounsfield (1919-2004): The man who revolutionized neuroimaging. *Ann Indian Acad Neurol*. 2016;19:448-450.
9. Petrik V, Apok V, Britton JA, et al. Godfrey Hounsfield and the dawn of computed tomography. *Neurosurgery*. 2006;58:780-787; discussion 780-787.
10. Cormack AM. Nobel Lecture NobelPrize.org: Nobel Prize Outreach AB 2024; 1979
11. Fleischmann D, Boas FE. Computed tomography--old ideas and new technology. *Eur. Radiol*. 2011;21:510-517.
12. Mannil M, Saltybaeva N. Basics of Computed Tomography. In: Mannil M, Winklhofer SFX, editors. *Neuroimaging Techniques in Clinical Practice: Physical Concepts and Clinical Applications*. Cham: Springer International Publishing; 2020. p. 31-43.
13. Mahesh M. The AAPM/RSNA Physics Tutorial for Residents. *Radiographics*. 2002;22:949-962.
14. Nüsslin F. Wilhelm Conrad Röntgen: The scientist and his discovery. *Phys. Med*. 2020;79:65-68.
15. Carlsson S. *Radiologi. Radiologi: Studentlitteratur AB, Lund; 2008. p. 19-101.*

16. Taubmann O, Berger M, Bögel M, et al. Computed Tomography. In: Maier A, Steidl S, Christlein V, Hornegger J, editors. *Medical Imaging Systems: An Introductory Guide*. Cham: Springer International Publishing; 2018. p. 147-189.
17. Dance DA. *Diagnostic Radiology Physics* [E-Book]. IAEA, Vienna: International Atomic Energy Agency; 2014.
18. Borges AP, Antunes C, Curvo-Semedo L. Pros and Cons of Dual-Energy CT Systems: "One Does Not Fit All". *Tomography*. 2023;9:195-216.
19. Forghani R, De Man B, Gupta R. Dual-Energy Computed Tomography: Physical Principles, Approaches to Scanning, Usage, and Implementation: Part 1. *Neuroimaging Clin. N. Am.* 2017;27:371-384.
20. Hounsfield GN. Nobel Lecture NobelPrize.org; Nobel Prize Outreach AB 2024; 1979
21. Seeram E. *Computed Tomography: Physical Principles, Patient Care, Clinical Applications, and Quality Control*. 5th ed: Saunders; 2022.
22. Flohr T, Ohnesorge B. Multi-slice CT Technology. In: Ohnesorge BM, Flohr TG, Becker CR, Knez A, Reiser MF, editors. *Multi-slice and Dual-source CT in Cardiac Imaging: Principles — Protocols — Indications — Outlook*. Berlin, Heidelberg: Springer Berlin Heidelberg; 2007. p. 41-69.
23. Romans LE. *Computed Tomography for Technologists*. 2 ed: Wolters Kluwer; 2019.
24. Tan CO, Kuppens D, Gupta R. Dual-Energy CT. In: Mannil M, Winklhofer SFX, editors. *Neuroimaging Techniques in Clinical Practice: Physical Concepts and Clinical Applications*. Cham: Springer International Publishing; 2020. p. 69-86.
25. Postma AA, Das M, Stadler AA, et al. Dual-Energy CT: What the Neuroradiologist Should Know. *Curr Radiol Rep*. 2015;3:16.
26. Chung R, Dane B, Yeh BM, et al. Dual-Energy Computed Tomography: Technological Considerations. *Radiol. Clin. North Am.* 2023;61:945-961.
27. Greffier J, Villani N, Defez D, et al. Spectral CT imaging: Technical principles of dual-energy CT and multi-energy photon-counting CT. *Diagn Interv Imaging*. 2023;104:167-177.
28. McCollough CH, Leng S, Yu L, et al. Dual- and Multi-Energy CT: Principles, Technical Approaches, and Clinical Applications. *Radiology*. 2015;276:637-653.
29. Große Hokamp N, Maintz D, Shapira N, et al. Technical background of a novel detector-based approach to dual-energy computed tomography. *Diagn. Interv. Radiol*. 2020;26:68-71.
30. Forghani R, De Man B, Gupta R. Dual-Energy Computed Tomography: Physical Principles, Approaches to Scanning, Usage, and Implementation: Part 2. *Neuroimaging Clin. N. Am.* 2017;27:385-400.
31. García-Figueiras R, Oleaga L, Broncano J, et al. What to Expect (and What Not) from Dual-Energy CT Imaging Now and in the Future? *J Imaging*. 2024;10.

32. Gaddam DS, Dattwyler M, Fleiter TR, et al. Principles and Applications of Dual Energy Computed Tomography in Neuroradiology. *Semin. Ultrasound. CT MR.* 2021;42:418-433.
33. Goldman LW. Principles of CT: Radiation Dose and Image Quality. *J. Nucl. Med. Technol.* 2007;35:213.
34. den Harder AM, Willemink MJ, Budde RP, et al. Hybrid and model-based iterative reconstruction techniques for pediatric CT. *AJR Am. J. Roentgenol.* 2015;204:645-653.
35. Willemink MJ, de Jong PA, Leiner T, et al. Iterative reconstruction techniques for computed tomography Part 1: Technical principles. *Eur. Radiol.* 2013;23:1623-1631.
36. Willemink MJ, Leiner T, de Jong PA, et al. Iterative reconstruction techniques for computed tomography part 2: initial results in dose reduction and image quality. *Eur. Radiol.* 2013;23:1632-1642.
37. Willemink MJ, Noël PB. The evolution of image reconstruction for CT-from filtered back projection to artificial intelligence. *Eur. Radiol.* 2019;29:2185-2195.
38. Maass C, Baer M, Kachelriess M. Image-based dual energy CT using optimized precorrection functions: a practical new approach of material decomposition in image domain. *Med. Phys.* 2009;36:3818-3829.
39. Tatsugami F, Higaki T, Nakamura Y, et al. Dual-energy CT: minimal essentials for radiologists. *Jpn J Radiol.* 2022;40:547-559.
40. Siegel MJ, Kaza RK, Bolus DN, et al. White paper of the society of computed body tomography and magnetic resonance on dual-energy ct, part 1: Technology and terminology. *J. Comput. Assist. Tomogr.* 2016;40:841-845.
41. Rassouli N, Etesami M, Dhanantwari A, et al. Detector-based spectral CT with a novel dual-layer technology: principles and applications. *Insights Imaging.* 2017;8:589-598.
42. Healthcare P. A scientific review of dual-energy and spectral computed tomography imaging 2020 2 December 2024.
43. Hounsfield GN. Picture quality of computed tomography. *AJR Am. J. Roentgenol.* 1976;127:3-9.
44. Barrett JF, Keat N. Artifacts in CT: Recognition and Avoidance. *Radiographics.* 2004;24:1679-1691.
45. Katsura M, Sato J, Akahane M, et al. Current and Novel Techniques for Metal Artifact Reduction at CT: Practical Guide for Radiologists. *Radiographics.* 2018;38:450-461.
46. Verdun FR, Racine D, Ott JG, et al. Image quality in CT: From physical measurements to model observers. *Phys. Med.* 2015;31:823-843.
47. Rozeik C, Kotterer O, Preiss J, et al. Cranial CT artifacts and gantry angulation. *J. Comput. Assist. Tomogr.* 1991;15:381-386.
48. Altman DG. Practical Statistics for Medical research. *Stat. Med.* 1991;10:1635-1636.
49. Strålsäkerhetsmyndigheten. Radiologiska undersökningar i Sverige under 2018.



<https://www.stralsakerhetsmyndigheten.se/publikationer/rapporter/stralskydd/>; 2020.

50. Prislister bild- och funktionsmedicin: Region Skåne <https://vardgivare.skane.se/patientadministration/avgifter-och-prislister/prislister-bild-funktionsmedicin/>; Region Skåne; 2024 [cited 2024 2 December].
51. Wardlaw JM, von Kummer R, Farrall AJ, et al. A large web-based observer reliability study of early ischaemic signs on computed tomography. The Acute Cerebral CT Evaluation of Stroke Study (ACCESS). PLoS ONE. 2010;5:e15757.
52. Mair G, Boyd EV, Chappell FM, et al. Sensitivity and specificity of the hyperdense artery sign for arterial obstruction in acute ischemic stroke. Stroke. 2015;46:102-107.
53. Oleaga L. Central Nervous System. eBook for Undergraduate Education in Radiology: European Society of Radiology; 2022.
54. Brant WE. Fundamentals of Diagnostic Radiology. 3rd ed: Lippincott Williams & Wilkins; 2006.
55. Birenbaum D, Bancroft LW, Felsberg GJ. Imaging in acute stroke. West J Emerg Med. 2011;12:67-76.
56. Keep RF, Andjelkovic AV, Xi G. Chapter 29 - Cytotoxic and Vasogenic Brain Edema. In: Caplan LR, Biller J, Leary MC, Lo EH, Thomas AJ, Yenari M, et al., editors. Primer on Cerebrovascular Diseases (Second Edition). San Diego: Academic Press; 2017. p. 145-149.
57. Han W, Song Y, Rocha M, et al. Ischemic brain edema: Emerging cellular mechanisms and therapeutic approaches. Neurobiol. Dis. 2023;178:106029.
58. Becker H, Desch H, Hacker H, et al. CT fogging effect with ischemic cerebral infarcts. Neuroradiology. 1979;18:185-192.
59. Ricarte IF, Pedroso JL, Carvalho FA, et al. The essential can be invisible to the eyes: the "fogging effect" phenomenon in the subacute stage of ischemic stroke. J Stroke Cerebrovasc Dis. 2013;22:e628-629.
60. Braileanu M, Weinberg BD, Hu R, et al. Appearance of cerebral infarct fogging on CT perfusion. Radiol Case Rep. 2019;14:889-893.
61. Barber PA, Demchuk AM, Zhang J, et al. Validity and reliability of a quantitative computed tomography score in predicting outcome of hyperacute stroke before thrombolytic therapy. The Lancet. 2000;355:1670-1674.
62. Kumar SS, N. Acute Ischemic Stroke: A Review of Imaging, Patient Selection, and Management in the Endovascular Era. Part I: Initial Management and Imaging. Journal of Clinical Interventional Radiology. 2018:155-168.
63. von Kummer R, Allen KL, Holle R, et al. Acute stroke: usefulness of early CT findings before thrombolytic therapy. Radiology. 1997;205:327-333.
64. Powers WJ, Rabinstein AA, Ackerson T, et al. Guidelines for the Early Management of Patients With Acute Ischemic Stroke: 2019 Update to the 2018 Guidelines for the Early Management of Acute Ischemic Stroke: A Guideline

- for Healthcare Professionals From the American Heart Association/American Stroke Association. *Stroke*. 2019;50:e344-e418.
65. Lin MP, Liebeskind DS. Imaging of Ischemic Stroke. *Continuum (Minneapolis, Minn)*. 2016;22:1399-1423.
  66. Simonsen CZ, Madsen MH, Schmitz ML, et al. Sensitivity of diffusion- and perfusion-weighted imaging for diagnosing acute ischemic stroke is 97.5%. *Stroke*. 2015;46:98-101.
  67. Khalil AA, Hohenhaus M, Kunze C, et al. Sensitivity of Diffusion-Weighted STEAM MRI and EPI-DWI to Infratentorial Ischemic Stroke. *PLoS ONE*. 2016;11:e0161416.
  68. Nagayama Y, Tanoue S, Oda S, et al. Metal Artifact Reduction in Head CT Performed for Patients with Deep Brain Stimulation Devices: Effectiveness of a Single-Energy Metal Artifact Reduction Algorithm. *AJNR Am. J. Neuroradiol*. 2020;41:231-237.
  69. Winklhofer S, Hinzpeter R, Stocker D, et al. Combining monoenergetic extrapolations from dual-energy CT with iterative reconstructions: reduction of coil and clip artifacts from intracranial aneurysm therapy. *Neuroradiology*. 2018;60:281-291.
  70. Bolstad K, Flatabø S, Aadnevik D, et al. Metal artifact reduction in CT, a phantom study: subjective and objective evaluation of four commercial metal artifact reduction algorithms when used on three different orthopedic metal implants. *Acta Radiol*. 2018;59:1110-1118.
  71. Hwang WD, Mossa-Basha M, Andre JB, et al. Qualitative Comparison of Noncontrast Head Dual-Energy Computed Tomography Using Rapid Voltage Switching Technique and Conventional Computed Tomography. *J. Comput. Assist. Tomogr*. 2016;40:320-325.
  72. Bonnemain B. History of Contrast Media: Celebrating the Centenary of the Use of Lipiodol in Radiology. *Erciyes Medical Journal*. 2021.
  73. Pollack HM. History of Iodinated Contrast Media. In: Thomsen HS, Muller RN, Mattrey RF, editors. *Trends in Contrast Media*. Berlin, Heidelberg: Springer Berlin Heidelberg; 1999. p. 3-19.
  74. Ambrose J. Computerized transverse axial scanning (tomography). 2. Clinical application. *Br. J. Radiol*. 1973;46:1023-1047.
  75. Christiansen C. X-ray contrast media--an overview. *Toxicology*. 2005;209:185-187.
  76. Pasternak JJ, Williamson EE. Clinical pharmacology, uses, and adverse reactions of iodinated contrast agents: a primer for the non-radiologist. *Mayo Clin. Proc*. 2012;87:390-402.
  77. Dekker HM, Stroomberg GJ, Prokop M. Tackling the increasing contamination of the water supply by iodinated contrast media. *Insights Imaging*. 2022;13:30.
  78. Modi KP, SA; Gupta, M. Contrast-Induced Nephropathy. <https://www.ncbi.nlm.nih.gov/books/NBK448066/>: Treasure Island (FL): StatPearls Publishing; 2023.

79. Huda W, Magill D, He W. CT effective dose per dose length product using ICRP 103 weighting factors. *Med. Phys.* 2011;38:1261-1265.
80. McCollough CH, Leng S, Yu L, et al. CT dose index and patient dose: they are not the same thing. *Radiology.* 2011;259:311-316.
81. Börjesson S, Håkansson M, Båth M, et al. A software tool for increased efficiency in observer performance studies in radiology. *Radiat. Prot. Dosimetry.* 2005;114:45-52.
82. Håkansson M, Svensson S, Zachrisson S, et al. ViewDEX: an efficient and easy-to-use software for observer performance studies. *Radiat. Prot. Dosimetry.* 2010;139:42-51.
83. Svalkvist A, Svensson S, Hagberg T, et al. Viewdex 3.0—Recent Development of a software Application Facilitating Assessment of Image Quality and Observer Performance. *Radiat. Prot. Dosimetry.* 2021;195:372-377.
84. Svalkvist A, Svensson S, Håkansson M, et al. Viewdex: A Status Report. *Radiat. Prot. Dosimetry.* 2016;169:38-45.
85. Goddard JK, Moran CJ, Cross DT, 3rd, et al. Absent relationship between the coil-embolization ratio in small aneurysms treated with a single detachable coil and outcomes. *AJNR. American journal of neuroradiology.* 2005;26:1916-1920.
86. Hansson J, Månsson LG, Båth M. Evaluation of VGC Analyzer by Comparison with Gold Standard ROC Software and Analysis of Simulated Visual Grading Data. *Radiat. Prot. Dosimetry.* 2021;195:378-390.
87. Hansson J, Månsson LG, Båth M. The Validity of Using ROC Software for Analysing Visual Grading Characteristics Data: An Investigation based in the Novel Sooftware VGC Analyzer. *Radiat. Prot. Dosimetry.* 2016;169:54-59.
88. Båth M, Hansson J. VGC Analyzer: A Software for Statistical Analysis of Fully Crossed Multiple-Reader Multiple-Case Visual grading Characteristics Studies. *Radiat. Prot. Dosimetry.* 2016;169:46-53.
89. Båth M, Månsson LG. Visual grading characteristics (VGC) analysis: a non-parametric rank-invariant statistical method for image quality evaluation. *Br. J. Radiol.* 2007;80:169-176.
90. Noël PB, Fingerle AA, Renger B, et al. Initial Performance Characterization of a Clinical Noise-Suppressing Reconstruction Algorithm for MDCT. *Am. J. Roentgenol.* 2011;197:1404-1409.
91. Willemink MJ, Takx RA, de Jong PA, et al. Computed tomography radiation dose reduction: effect of different iterative reconstruction algorithms on image quality. *J. Comput. Assist. Tomogr.* 2014;38:815-823.
92. Löve A, Olsson ML, Siemund R, et al. Six iterative reconstruction algorithms in brain CT: a phantom study on image quality at different radiation dose levels. *Br. J. Radiol.* 2013;86:20130388.
93. Smith-Bindman R, Wang Y, Chu P, et al. International variation in radiation dose for computed tomography examinations: prospective cohort study. *BMJ.* 2019;364:k4931.

94. Riederer I, Fingerle AA, Baum T, et al. Acute infarction after mechanical thrombectomy is better delineable in virtual non-contrast compared to conventional images using a dual-layer spectral CT. *Scientific reports*. 2018;8:9329-9329.
95. Zhao X-M, Wang M, Wu R-Z, et al. Dual-layer spectral detector CT monoenergetic reconstruction improves image quality of non-contrast cerebral CT as compared with conventional single energy CT. *Eur. J. Radiol*. 2018;103:131-138.
96. Pomerantz SR, Kamalian S, Zhang D, et al. Virtual Monochromatic Reconstruction of Dual-Energy Unenhanced Head CT at 65–75 keV Maximizes Image Quality Compared with Conventional Polychromatic CT. *Radiology*. 2013;266:318-325.
97. Neuhaus V, Abdullayev N, Große Hokamp N, et al. Improvement of Image Quality in Unenhanced Dual-Layer CT of the Head Using Virtual Monoenergetic Images Compared With Polyenergetic Single-Energy CT. *Invest. Radiol*. 2017;52:470-476.
98. Große Hokamp N, Hellerbach A, Gierich A, et al. Reduction of Artifacts Caused by Deep Brain Stimulating Electrodes in Cranial Computed Tomography Imaging by Means of Virtual Monoenergetic Images, Metal Artifact Reduction Algorithms, and Their Combination. *Invest. Radiol*. 2018;53:424-431.
99. Jabas A, Abello Mercado MA, Altmann S, et al. Single-Energy Metal Artifact Reduction (SEMAR) in Ultra-High-Resolution CT Angiography of Patients with Intracranial Implants. *Diagnostics (Basel)*. 2023;13.
100. Zopfs D, Lennartz S, Pennig L, et al. Virtual monoenergetic images and post-processing algorithms effectively reduce CT artifacts from intracranial aneurysm treatment. *Scientific Reports*. 2020;10:6629.
101. Selles M, Stuivenberg VH, Wellenberg RHH, et al. Quantitative analysis of metal artifact reduction in total hip arthroplasty using virtual monochromatic imaging and orthopedic metal artifact reduction, a phantom study. *Insights Imaging*. 2021;12:171.
102. Choo HJ, Lee SJ, Kim DW, et al. Comparison of the Quality of Various Polychromatic and Monochromatic Dual-Energy CT Images with or without a Metal Artifact Reduction Algorithm to Evaluate Total Knee Arthroplasty. *Korean J. Radiol*. 2021;22:1341-1351.
103. Bamberg F, Dierks A, Nikolaou K, et al. Metal artifact reduction by dual energy computed tomography using monoenergetic extrapolation. *Eur. Radiol*. 2011;21:1424-1429.
104. Guggenberger R, Winklhofer S, Osterhoff G, et al. Metallic artefact reduction with monoenergetic dual-energy CT: systematic ex vivo evaluation of posterior spinal fusion implants from various vendors and different spine levels. *Eur. Radiol*. 2012;22:2357-2364.
105. Johansen CB, Martinsen ACT, Enden TR, et al. The potential of iodinated contrast reduction in dual-energy CT thoracic angiography; an evaluation of image quality. *Radiography (Lond)*. 2022;28:2-7.

106. Shuman WP, Chan KT, Busey JM, et al. Dual-energy CT Aortography with 50% Reduced Iodine Dose Versus Single-energy CT Aortography with Standard Iodine Dose. *Acad. Radiol.* 2016;23:611-618.
107. Saleh M, Mujtaba B, Jensen C, et al. Feasibility of half the recommended dose of IV contrast in DECT: image quality evaluation and diagnostic acceptability in cancer patients. *Clin. Imaging.* 2022;88:59-65.
108. Yuan R, Shuman WP, Earls JP, et al. Reduced iodine load at CT pulmonary angiography with dual-energy monochromatic imaging: comparison with standard CT pulmonary angiography--a prospective randomized trial. *Radiology.* 2012;262:290-297.
109. Guerrini S, Zanoni M, Sica C, et al. Dual-Energy CT as a Well-Established CT Modality to Reduce Contrast Media Amount: A Systematic Review from the Computed Tomography Subspecialty Section of the Italian Society of Radiology. *J Clin Med.* 2024;13.
110. Katzberg RW. "Acute reactions to urographic contrast medium: incidence, clinical characteristics, and relationship to history of hypersensitivity states"--a commentary. *AJR Am. J. Roentgenol.* 2008;190:1431-1432.
111. Koepfel DR, Boehm IB. Shortage of iodinated contrast media: Status and possible chances - A systematic review. *Eur. J. Radiol.* 2023;164:110853.
112. Phan CM, Yoo AJ, Hirsch JA, et al. Differentiation of hemorrhage from iodinated contrast in different intracranial compartments using dual-energy head CT. *AJNR Am. J. Neuroradiol.* 2012;33:1088-1094.
113. Tijssen MP, Hofman PA, Stadler AA, et al. The role of dual energy CT in differentiating between brain haemorrhage and contrast medium after mechanical revascularisation in acute ischaemic stroke. *Eur. Radiol.* 2014;24:834-840.
114. Kessner R, Sommer J, Große Hokamp N, et al. Virtual versus true non-contrast images of the brain from spectral detector CT: comparison of attenuation values and image quality. *Acta Radiol.* 2023;64:776-783.
115. Bucolo GM, Ascenti V, Barbera S, et al. Virtual Non-Contrast Spectral CT in Renal Masses: Is It Time to Discard Conventional Unenhanced Phase? *J Clin Med.* 2023;12.
116. Song I, Yi JG, Park JH, et al. Virtual Non-Contrast CT Using Dual-Energy Spectral CT: Feasibility of Coronary Artery Calcium Scoring. *Korean J. Radiol.* 2016;17:321-329.
117. Lee MH, Park HJ, Kim JN, et al. Virtual non-contrast images from dual-energy CT angiography of the abdominal aorta and femoral arteries: comparison with true non-contrast CT images. *Br. J. Radiol.* 2022;95:20220378.
118. Vlahos I, Jacobsen MC, Godoy MC, et al. Dual-energy CT in pulmonary vascular disease. *Br. J. Radiol.* 2022;95:20210699.
119. Fransson V, Mellander H, Wasselius J, et al. Detection of Perfusion Deficits in Multiphase Computed Tomography Angiography-A Stroke Imaging Technique Based on Iodine Mapping on Spectral Computed Tomography: Initial Findings. *J. Comput. Assist. Tomogr.* 2021;45:618-624.

120. Uhrig M, Simons D, Bonekamp D, et al. Improved detection of melanoma metastases by iodine maps from dual energy CT. *Eur. J. Radiol.* 2017;90:27-33.
121. Willemink MJ, Persson M, Pourmorteza A, et al. Photon-counting CT: Technical Principles and Clinical Prospects. *Radiology.* 2018;289:293-312.
122. Brady SL. Implementation of AI image reconstruction in CT-how is it validated and what dose reductions can be achieved. *Br. J. Radiol.* 2023;96:20220915.

